

THESIS

THE CONTRIBUTION OF ^{238}U AND ^{232}Th TO RADIATION DOSE AND RISK
FROM FLY ASH EFFLUENT OF COAL-FIRED POWER PLANTS

Submitted by

Felicity Cunningham Beckfield

Department of Environmental and Radiological Health Sciences

In partial fulfillment of the requirements

For the Degree of Master of Science

Colorado State University

Fort Collins, Colorado

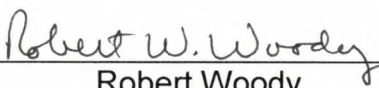
Spring 2010

COLORADO STATE UNIVERSITY

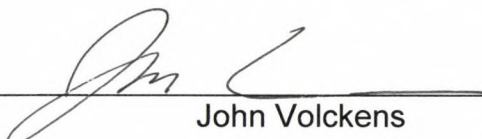
MARCH 9, 2010

WE HEREBY RECOMMEND THAT THE THESIS PREPARED
UNDER OUR SUPERVISION BY FELICITY CUNNINGHAM BECKFIELD
ENTITLED THE CONTRIBUTION OF ^{238}U AND ^{232}Th TO RADIATION DOSE
AND RISK FROM FLY ASH EFFLUENT OF COAL-FIRED POWER PLANTS
BE ACCEPTED AS FULFILLING IN PART REQUIREMENTS FOR THE
DEGREE OF MASTER OF SCIENCE.

Committee on Graduate Work




Robert Woody



John Volckens



Advisor: Thomas Johnson



Department Head: Jac Nickoloff

ABSTRACT OF THESIS

THE CONTRIBUTION OF ^{238}U AND ^{232}Th TO RADIATION DOSE AND RISK FROM FLY ASH EFFLUENT OF COAL-FIRED POWER PLANTS

The goal of this project was to determine the activity concentrations of ^{238}U and ^{232}Th emitted from a coal-fired power plant that could potentially impact human health and the environment. The activity concentration of ^{238}U and ^{232}Th in fly ash was used to estimate effluent uranium and thorium. The estimate of effluent activity was then used to model radiation dose and evaluate any associated increase in cancer risk to employees working in the plant and individuals living near the plant. Grab samples of fly ash were obtained and manually fractionated using the soil sizing techniques of sieving and pipetting. The respective samples were counted using alpha spectroscopy to determine the activity concentrations of ^{238}U and ^{232}Th . Whole body dose was calculated using 10 CFR 20 Appendix B annual limits on intake (ALI). The alpha emissions from ^{238}U and ^{232}Th are of particular interest as they are significant contributors to dose in the lungs and other tissues due to their high relative biologic effectiveness and short range. The results of this study indicate that fly ash contains both ^{238}U and ^{232}Th but is not a radioactive substance as defined by the IAEA transportation safety

standards and Title 49 of the Code of Federal Regulations. Although the relative concentration of radionuclides in the fly ash of this study is quite low, it is still possible for individuals to receive a measurable dose. Exceeding occupational and public dose limits would require inhalation of approximately 1-1000 kg of fly ash for ^{238}U and approximately 50 g to 20 kg for ^{232}Th . The highest CEDE (ICRP 30) per unit mass incurred by inhalation of fly ash was class W ^{232}Th (1.81 mrem g^{-1}), while class W ^{238}U had the lowest CEDE per unit mass ($3.32 \text{ } \mu\text{rem g}^{-1}$). The general relationship between activity concentration of ^{238}U and ^{232}Th found using data from radiochemical analysis and particle size suggest that activity concentration increases with increasing particle size. However the relationship between activity concentration and particle size found in the literature suggests that activity concentration increases with decreasing particle size. The accompanying health risk from ^{238}U and ^{232}Th in fly ash is predicted to be less than 10^{-5} percent.

Felicity Cunningham Beckfield
Department of Environmental and Radiological Health Sciences
Colorado State University
Fort Collins, CO 80523
Spring 2010

ACKNOWLEDGEMENTS

I would like to thank my committee Drs. Johnson, Volckens, and Woody. Thank you, Dr. Pinder, for all your help with my data analysis. I will never forget your kindness and humor. You made me laugh even during the toughest of times. A very special thank you goes to Aimee Oke for all her emotional and professional support through this process. Without you Aimee, I wouldn't have graduated. Thank you, Julie Asmus, for your administrative expertise. You hold this department together! Thank you, Marion Dahlgren, for all your help during the grant proposal process, you were a God send. I am indebted to the NIOSH Mountain and Plains Education and Research Center for funding my graduate education. I promise to be worthy of the investment. This project was funded by grant number 1T42OH009229-01 from CDC NIOSH Mountain and Plains Education and Research Center.

To the Health Physics Class of 2009 (you know who you are), thanks for all the necessary distractions. You all kept me sane my first year. I've missed you! To Brian Lane, thanks for always listening, buddy. Good luck with your future endeavors. To Elizabeth Gillenwalters, Cheri Hall, Nicole Martinez, Katy Swancutt, Niko Roche, and Ward Mayzad, wow, you are some of the funniest people I have ever met. Thank you for being there, listening to my problems, and watching me laugh and cry...at the same time. I will never forget your friendship and kindness.

To Mom and Dad, thank you. Thank you for teaching me how to be the person I am today. I couldn't have done this without your support.

Lastly, I want to thank my little family. Connor puppy, you're the greatest friend anyone could ever ask for. Thanks for being so excited to see me when I get home. Richie my love, you have stuck by me through thick and thin. If it weren't for you and your support, I would have never made it. I love you.

TABLE OF CONTENTS

ABSTRACT OF THESIS	iii
ACKNOWLEDGEMENTS	v
TABLE OF CONTENTS	vii
LIST OF TABLES	ix
LIST OF FIGURES	xi
LIST OF ABBREVIATIONS	xii
Chapter 1: Introduction and Background	1
1.1 Objectives	1
1.2 Coal	2
1.2.1 <i>Properties of Coal</i>	2
1.2.2 <i>Powder River Basin Coal</i>	4
1.3 Coal-Fired Power Plants	7
1.3.1 <i>History</i>	7
1.3.2 <i>Operation</i>	7
1.4 Power Plant Description	10
1.5 Conditions within the Stack	11
1.6 Debate Regarding the Radioactivity and Risks of Coal Fly Ash	11
1.5 Respirable Particulate Matter	18
Chapter 2: Materials and Methods	20
2.1 Sampling for Radioactivity	20
2.1.1 <i>Fly Ash Grab Sampling and Gamma Spectroscopy</i>	20
2.1.2 <i>Determination of Limit of Detection for Gross Alpha and Beta Counting</i>	21
2.2 Study Design	23
2.2.1 <i>Fly Ash Size Fractionation</i>	23
2.2.2 <i>Gross Alpha and Beta Counting</i>	24
2.2.3 <i>Radiochemical Analysis</i>	25
2.2.4 <i>Determination of Whole Body Dose from Inhalation Exposure</i>	27
Chapter 3: Data and Analysis	31
3.1 Gamma Spectroscopy of Fly Ash	31
3.2 Gross Alpha and Beta Limit of Detection for Fly Ash Mass and Calibration Curves	33
3.3 Count Rate vs. Sample Mass Relationship and Statistics	37
3.3.1 <i>Gross Alpha Count Rate vs. Sample Mass Relationship</i>	37
3.3.1a <i>Linear Transformation</i>	37
3.3.1b <i>Logarithmic Transformation</i>	39
3.3.2 <i>Gross Beta Count Rate vs. Sample Mass Relationship</i>	40
3.4 Fly Ash Particle Size Distribution	42
3.5 Gross Alpha and Beta Activity Concentration vs. Particle Size	42
3.6 Radiochemical Analysis Data	44
3.6.1 <i>Mass Spectroscopy Results</i>	44
3.6.2 <i>Alpha Spectroscopy Results</i>	45
3.7 ²³⁸U and ²³²Th Activity Concentration vs. Particle Size	46

3.8	Activity Median Aerodynamic Diameter	48
3.9	Dose Based on Inhaled Fly Ash Particulate Matter	48
3.9.1	<i>Calculating Committed Effective Dose Equivalent</i>	48
3.9.2	<i>Dose Received by Inhaled Mass</i>	54
Chapter 4: Discussion		57
4.1	Discussion of Fly Ash Particle Size Distribution	57
4.2	Discussion of Radiochemical Analysis	57
4.3	Uncertainties in the Dose Calculation	58
4.4	Explanation for the Trends in the Gross Alpha and Beta Count Rate vs. Mass Data	60
4.4.1	<i>Explanation for the Trends in the Gross Alpha Count Rate vs. Mass</i>	60
4.4.2	<i>Explanation for the Trends in the Gross Beta Count Rate vs. Mass</i>	61
4.4.3	<i>Gross Alpha and Beta Counting for Dose Assessment</i>	62
4.5	Activity Concentration vs. Particle Size Relationship	62
4.6	Dose Assessment and Risk from Inhalation of Fly Ash Material	63
4.6.1	<i>Dose Assessment and Risk using Data Provided by Radiochemical Analysis</i>	63
4.6.2	<i>Dose Assessment and Risk using Data Provided by Radiochemical Analysis Accounting for Uncertainties</i>	64
4.7	Further Research	65
4.8	Conclusion	67
References		69
Appendix A		74
Appendix B		76
Appendix C		78
Appendix D		83
Appendix E		88
Appendix F		93
Appendix G		95
Appendix H		96

LIST OF TABLES

Table 1.1: Gross Calorific Value by Coal Rank	4
Table 1.2: Properties of PRB coal in the Wyodak-Anderson coal zone.....	5
Table 1.3: Arithmetic mean concentration (ppm) of elements which are of environmental concern in Wyodak-Anderson study and release rates upon combustion.....	5
Table 1.4: US EPA Average emission rates from coal-fired power generation	8
Table 1.5: Decay chain progeny present in coal, bottom ash, and fly ash	12
Table 1.6: Concentration (ppm) of elemental uranium and thorium in coal ...	13
Table 1.7: Concentration (ppm) of elemental uranium and thorium in coal fly ash	14
Table 1.8: Activity concentration in coal for ^{238}U and ^{232}Th	15
Table 1.9: Activity concentration in fly ash for ^{238}U and ^{232}Th	15
Table 1.10: Emission rates of ^{238}U and ^{232}Th from CFPPs.....	16
Table 1.11: Emission rates of ^{238}U and ^{232}Th from CFPPs.....	17
Table 2.2: Occupational values and effluent concentrations for ^{238}U	29
Table 2.3: Occupational values and effluent concentrations for ^{232}Th	30
Table 3.1: Peak identification output from spectroscopy software	32
Table 3.2: Detectable count rate above background for alpha particles.....	34
Table 3.3: Detectable count rate above background for beta particles	35
Table 3.2: Particle size distribution of fly ash samples	42
Table 3.4: ICPMS results for elemental U and Th.....	44
Table 3.6: Activity concentration of ^{238}U and ^{232}Th in raw fly ash.....	45
Table 3.7: Activity concentration in each size fraction for ^{238}U	46
Table 3.8: Activity concentration in each size fraction for ^{232}Th	46
Table 3.9: Changes in deposition fraction with varying AMAD	48
Table 3.10: ICRP 30 CDEs for ^{238}U , class D, W, Y	50
Table 3.11: ICRP 60 CDEs ^{238}U , class F(D), M(W), S(Y).....	51
Table 3.12: ICRP 30 CDEs ^{232}Th , class W, Y	52
Table 3.13: ICRP 60 CDEs ^{232}Th , class M(W), S(Y)	53
Table 3.14: CEDE by radionuclide, model, and class	53
Table 3.15: Average concentrations of ^{238}U and ^{232}Th	54
Table 3.16: Dose per unit mass by nuclide, model, and class	56
Table 4.1: Mass median diameters found in the literature for stack fly ash...	57
Table 4.2: Ratios of Th:U in fly ash from the literature	58
Table 4.3: Changes in deposition fraction using re-calculated AMAD.....	59
Table 4.4: CEDE by radionuclide, model, and class	59
Table 4.5: Dose per unit mass by nuclide, model, and class	60
Table 4.6: Detriment coefficients for stochastic effects	63
Table 4.7: ICRP 30 increased risk from inhalation of 1 g of fly ash.....	64
Table 4.8: ICRP 60 increased risk from inhalation of 1 g of fly ash.....	64
Table 4.9: ICRP 30 increased risk of stochastic effect from inhalation of 1 g of fly ash accounting for size uncertainties.....	65

Table 4.10: ICRP 60 increased risk of stochastic effect from inhalation of 1 g of fly ash accounting for size uncertainties.....	65
Table A.1: Mass inhaled to reach public and occupational limits, ICRP 30... 74	74
Table A.2: Dose responsible for x mass in grams to be inhaled, ICRP 30....	74
Table A.3: Mass inhaled to reach public and occupational limits, ICRP 60... 74	74
Table A.4: Dose responsible for x mass in grams to be inhaled, ICRP 30....	75
Table B.1: Mass inhaled to reach public and occupational limits with size correction, ICRP 30.....	76
Table B.2: Dose responsible for x mass in grams to be inhaled with size correction, ICRP 30.....	76
Table B.3: Mass inhaled to reach public and occupational limits with size correction, ICRP 60.....	76
Table B.4: Dose responsible for x mass in grams to be inhaled with size correction, ICRP 60.....	77
Table G.1: Size adjustment calculations for ^{238}U	95
Table G.2: Size adjustment calculations for ^{232}Th	95

LIST OF FIGURES

Figure 1.1: The coal formation process, reprinted with permission from Kentucky Geological Survey	2
Figure 1.2: Pictorial representation of coal rank, reprinted with permission from Kentucky Geological Survey	3
Figure 1.3: Wyodak-Anderson Study Limit including concentrations of elemental Uranium	6
Figure 1.4: Pictorial representation of coal combustion process	9
Figure 2.1: Decay chains provided by the USGS	21
Fig. 3.1: Relationship between gross alpha net count rate and mass with a log transformation	36
Fig. 3.2: Relationship between gross beta net count rate and mass with a log transformation	36
Figure 3.3: Alpha Count Rate vs. Sample Mass, linear transformation with error bars representing one standard deviation	37
Figure 3.4: Non-linear regression of alpha count rate vs. mass data, linear transformation	38
Figure 3.5: Residual plot for alpha count rate vs. mass data, linear transformation	39
Figure 3.6: Residual plot for alpha count rate vs. mass data, log transformation	40
Figure 3.7: Residual plot for beta count rate vs. mass data, log transformation	41
Fig. 3.8: Relationship between gross alpha activity concentration in fly ash (pCi g^{-1}) and particle aerodynamic diameter (μm) with error bars representing one standard deviation	43
Fig. 3.9: Relationship between gross beta activity concentration in fly ash (pCi g^{-1}) and particle aerodynamic diameter (μm) with error bars representing one standard deviation	44
Figure 3.10: ^{238}U activity concentration vs. aerodynamic diameter for alpha spectroscopy data with error bars representing two standard deviations	47
Figure 3.11: ^{232}Th activity concentration vs. aerodynamic diameter for alpha spectroscopy data with error bars representing two standard deviations	47

LIST OF ABBREVIATIONS

ALI	annual limit on intake
AMAD	activity median aerodynamic diameter
BEIR	Biological Effects of Ionizing Radiation
Bq	Bequerel
CCP	coal combustion products
CDE	committed dose equivalent
CEDE	committed effective dose equivalent
CFPP	coal-fired power plant
Ci	Curie
cps	counts per second
CSU	Colorado State University
D	days
EIA	Energy Information Administration
EPA	Environmental Protection Agency
ESP	electrostatic precipitator
F	fast
GSD	geometric standard deviation
GWe	gigawatt electric
IAEA	International Atomic Energy Agency
ICPMS	inductively coupled plasma mass spectroscopy
ICRP	International Commission on Radiological Protection
ISO	International Standards Organization
M	medium
MDC	minimum detectable concentration
mg	milligram
MMAD	mass median aerodynamic diameter
NALI	non stochastic annual limit on intake
NORM	naturally occurring radioactive material
NP	nasopharyngeal
P	pulmonary
PM	particulate matter
ppm	parts per million
PRB	Powder River Basin
rem	radiation equivalent man
S	slow
SALI	stochastic annual limit on intake
Sv	Sievert
TB	tracheobronchial
TENORM	technologically enhanced naturally occurring radioactive material
W	weeks
Y	years

Chapter 1: Introduction and Background

1.1 Objectives

Radiation emission resulting from coal combustion has been a subject of interest since the 1970s.¹⁻¹² All coal contains radioactive isotopes, especially uranium, but the most important detail to identify about the coal is how much radioactivity the fly ash contains. In the state of Colorado, most electricity is generated via coal combustion. Colorado's coal-fired power plants often use coal that is mined in the Powder River Basin in the northeastern portion of Wyoming and southeastern portion of Montana.¹³

Upon release from a stack or chimney, coal combustion effluent is dispersed into the atmosphere. After dispersal into the atmosphere fly ash can be an inhalation hazard to the workers and the public. The fly ash removed by pollution control equipment is frequently sent to a landfill where resuspension may occur and act as a separate source of radioactive materials.

The intent of this study is to identify the radionuclides in fly ash. Additional goals are to quantify the concentration of radioactivity, by mass for ^{238}U and ^{232}Th , of the fly ash emitted from a coal-fired power plant. The activity concentration of ^{238}U and ^{232}Th was used to determine the amount of particulate matter (PM) mass an employee of the plant or a member of the nearby public would have to inhale to meet the regulatory limits for the

committed effective dose equivalent (CEDE).¹⁴ Risks due to the inhalation of fly ash material were also determined.

1.2 Coal

1.2.1 Properties of Coal

Coal is a fossil fuel, mostly comprised of decomposed vegetative matter (or peat), which over time has undergone bacterial decay, heat, and compaction or pressure.^{15, 16}

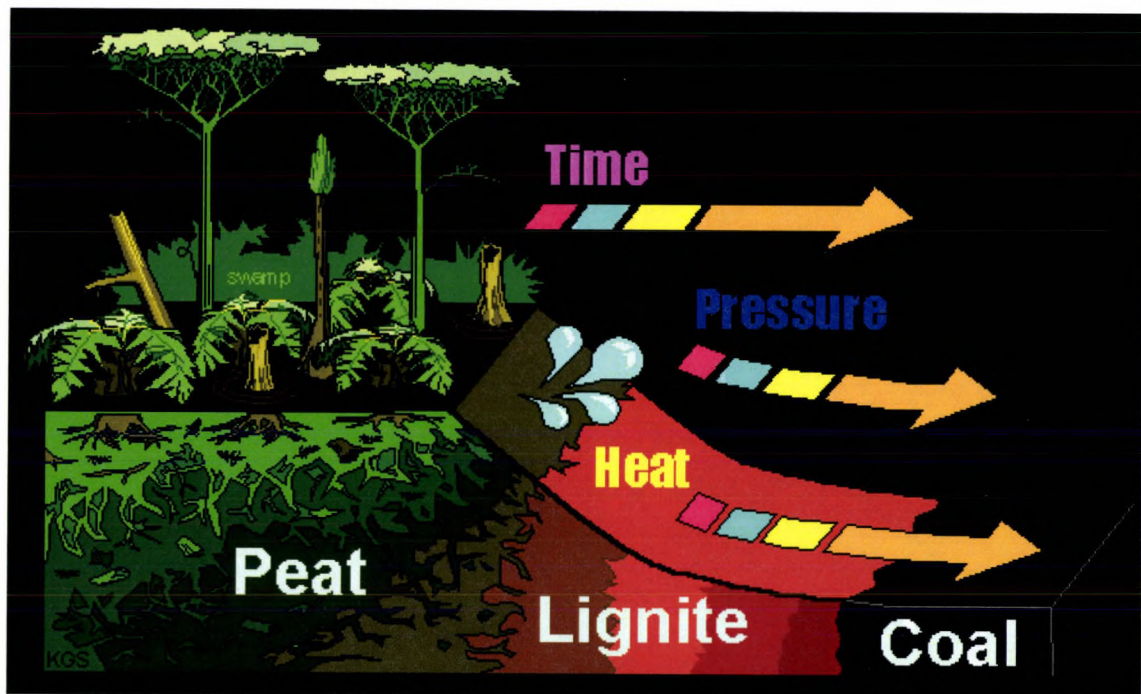


Figure 1.1: The coal formation process, reprinted with permission from Kentucky Geological Survey

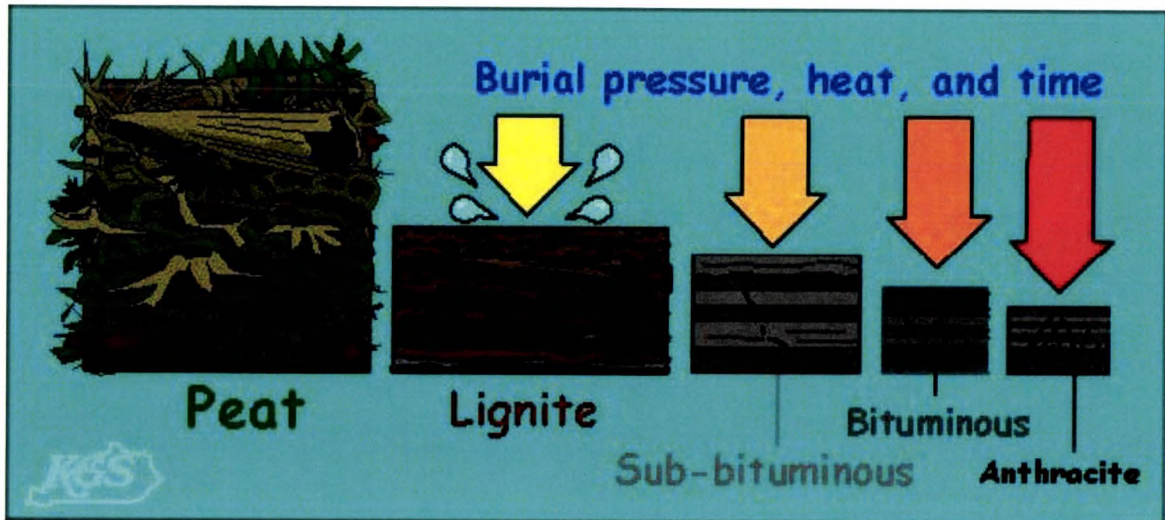


Figure 1.2: Pictorial representation of coal rank, reprinted with permission from Kentucky Geological Survey

Coal ranking classifies the degree of alteration that occurs as coal matures.¹⁷ Lignite is the lowest ranking coal in terms of energy content and is the least mature, followed by sub-bituminous. These low-rank coals have lower energy content due to their lower carbon content, are lighter in color (brown), and have higher moisture levels. Rank increases proportionally with time, heat and pressure. High ranking coals, such as bituminous and anthracite coals, contain more carbon (thus higher energy content), have lower moisture content, and have a darker, shinier appearance.

Table 1.1: Gross Calorific Value by Coal Rank¹⁸

Coal Rank	Gross Calorific Value (MJ/kg)
Peat	14.7
Brown Coal (lignite)	23.0
Sub-bituminous	33.5
High Volatile Bituminous	35.6
Medium Volatile Bituminous	36.0
Low Volatile Bituminous	36.4
Semi-anthracite	36.0
Anthracite	35.2

1.2.2 Powder River Basin Coal

Powder River Basin (PRB) is the chief coal-producing area in the coal deposit referred to as the Northern Great Plains Province and is located in northeastern Wyoming and southeastern Montana.¹⁸ It produces 43% of the USA's coal.¹⁹ The coal from this region is classified as sub-bituminous and its low sulfur content is environmentally attractive.¹⁸ Sub-bituminous coal has a dark brown to black color, has loose pore structure, and has more oxygen content than older coals (i.e. bituminous and anthracite).^{18, 20} In addition to its low sulfur content, PRB coal has a lower heating value, resulting from the higher moisture and oxygen content; higher volatility; and lower fusion temperature than other commonly burned coal (i.e. bituminous, anthracite) (Table 1.1).

The Bureau of Land Management reported that a total of 446.5 million tons of PRB coal were produced in Wyoming in 2008.²¹ A USGS study of the Wyodak-Anderson coal zone (Figure 1.3) was conducted by Stricker and Ellis. The study details are contained in Table 1.2.²²

Table 1.2: Properties of PRB coal in the Wyodak-Anderson coal zone²²

Property	Content
Moisture, %	27.66
Ash, %	6.44
Total Sulfur, %	0.48
Calorific Value, Btu/lb	8,220
Pounds of SO ₂ per million Btu	1.24

The same study also reported the arithmetic mean concentration (in parts per million) of elements found in the coal from 23 mines in the PRB. Those of environmental concern are listed in Table 1.3. These values are based on 446.5 million tons consumed per year with 6.44% ash content and 1% release rate after PM removal.

Table 1.3: Arithmetic mean concentration (ppm) of elements which are of environmental concern in Wyodak-Anderson study and release rates upon combustion

Element	Concentration (ppm)	Release Rates upon Combustion (tons yr ⁻¹)
Arsenic	2.6	0.75
Beryllium	0.54	0.16
Cadmium	0.21	0.06
Chromium	6.1	1.75
Cobalt	1.9	0.55
Lead	3.0	0.86
Manganese	26.0	7.48
Mercury	0.13	0.04
Nickel	4.6	1.32
Selenium	1.1	0.32
Uranium	1.3	0.37

However, another USGS study, at an Indiana CFPP, reported the mean concentration of uranium and thorium in PRB coal to be 8.9 ppm and 22 ppm respectively.²³ Coal from the PRB is utilized by power plants in 26 states.

Figure 1.3 is a map that represents the uranium concentration in the Wyodak-

Anderson coal in the PRB. The uranium found in coal is in both the mineral and organic fractions and the thorium is found in phosphate minerals like monazite or apatite.

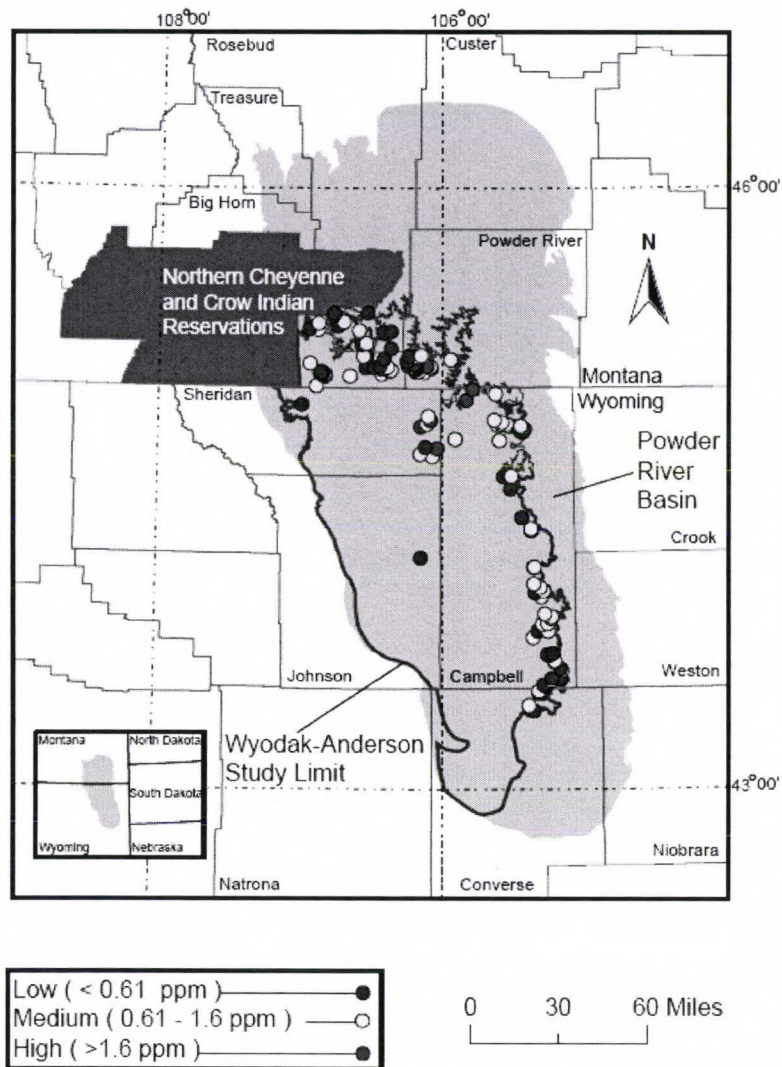


Figure 1.3: Wyodak-Anderson Study Limit including concentrations of elemental Uranium²²

1.3 Coal-Fired Power Plants

1.3.1 History

Coal is the most abundant and has the longest history of all fossil fuels. It was used by primitive cultures for heat and there has been archeological evidence that the Romans, while in England, used it between the years of 100-200 AD.²⁴ In the 1700s, the English discovered that coal was a better combustion fuel than wood charcoal for energy production, which was essential for providing the massive energy requirements for the Industrial Revolution. In December 1952, London, England experienced an unseasonably cold winter, thus households burned more coal for warmth. The resulting pollution yielded PM₁₀ concentrations ranging between 3,000-14,000 µg m⁻³ which was 50 times higher than the normal levels of the time.²⁵ Approximately 12,000 deaths resulted from this incident.

1.3.2 Operation

Coal was used to generate electricity for the first time in the 1880s. Coal power plants are now the greatest producer of electrical power in the United States. According to the Energy Information Administration (EIA), from April 2008 – April 2009, coal-fired power plants produced 46% of the United States' electricity.²⁶

The environmental impacts of coal combustion have greatly affected the world. In the US, power plants are regulated by federal and state laws to protect the environment as well as human health.¹⁶ Coal combustion yields

the following air emissions: carbon dioxide (CO₂), sulfur dioxide (SO₂), nitrogen oxides (NO_x), mercury, and PM. On average, the US emission rates from coal-fired power generation are listed in Table 1.4.¹⁶

Table 1.4: US EPA Average emission rates from coal-fired power generation

Emission	Emission Rate (lbs MWh⁻¹)
CO ₂	2,249
SO ₂	13
NO _x	6

In 2008, the annual electric power generation for coal in the US was 1,986 million MWh.¹³ It is still uncertain whether or not the fly ash emissions from coal-fired power plants contain significant amounts of radioactive PM and pose measurable risk.^{1-12, 27} In accordance with EPA guidelines, coal-fired power plants must have control devices (filtration mechanisms and scrubber systems) to reduce the emissions released as a result of coal combustion.¹⁶

Once mined, the coal is transported to the power plant, often by means of rail, truck, or barge, and is stockpiled at the power plant for future use.²⁸ When necessary, it is milled for use in the combustion chamber. Water is heated from the combustion process to create steam which turns the turbines to generate electricity. Coal combustion products (CCPs) are the waste products generated during the combustion process, which consist of fly ash, bottom ash, and combustion gases. CCPs must be removed from the system to reduce harmful air emissions. Emissions removal systems include the particulate removal system for fly ash removal (99% removal for fabric filtration and electrostatic precipitator),^{12, 29, 30} NO_x removal system (80-90% removal),³¹ and flue gas desulfurization unit for the removal of sulfates

(95%).¹⁸ The remaining components of the exhaust gases (traces of fly ash, CO₂, NO_x, and SO₂) are released into the atmosphere through the stack.

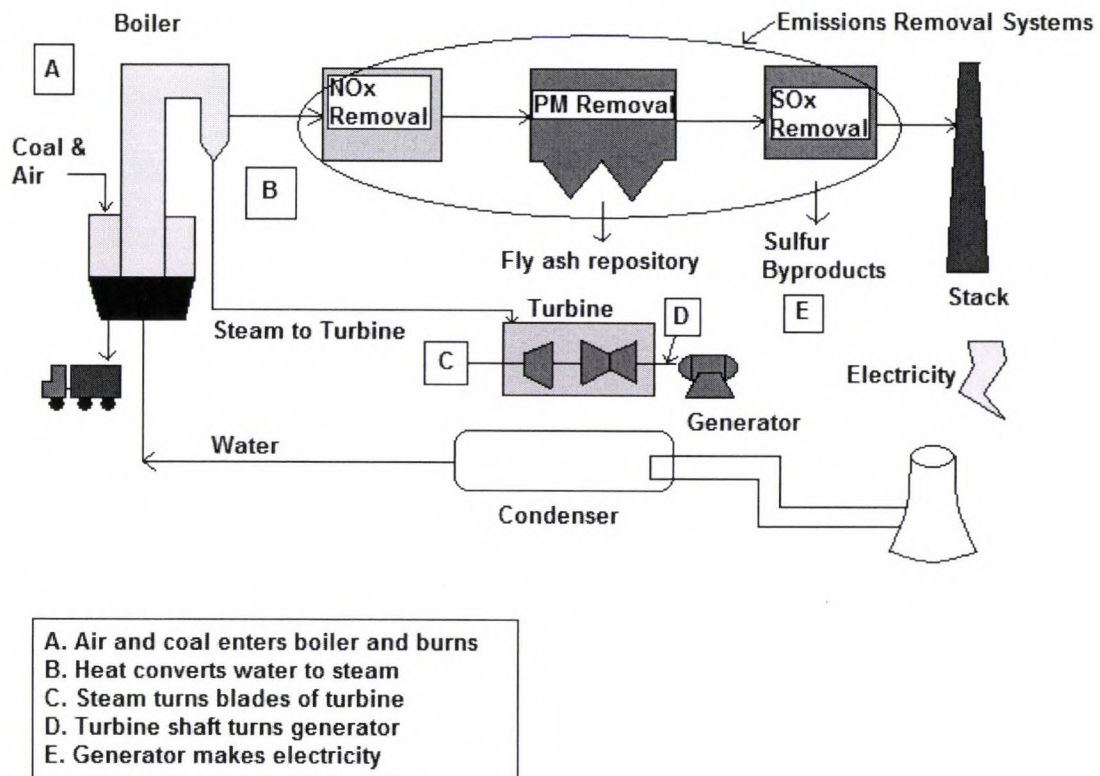


Figure 1.4: Pictorial representation of coal combustion process, recreated using information from the Coal Utilization Research Council³²

The combustion of coal yields two forms of ash: bottom ash and fly ash. The molten component of coal post combustion is cooled in a water bath, forming bottom ash. The bottom ash includes the coarse, heavier materials and slag.¹⁸ Fly ash is the lighter component found in the exhaust gases. The concentration of fly ash particulates are reduced by the PM filtration system (fabric filter or electrostatic precipitator) but a small fraction (1%) is released through the stack.

1.4 Power Plant Description

Measurements were taken at a coal fired power plant (the Plant) located in Colorado. The Plant is ranked as one of the cleanest power plants in the nation. The single unit facility operates at 270 MWe, which is enough electricity to serve 250,000 homes.⁴⁵ It is located on 4,400 acres of land and employs 100 people.²⁹

The Plant burns low-sulfur, PRB coal mined from the north central region of Wyoming. Coal trains arrive every other day with approximately 60-80 cars of coal carrying 100 tons each.^{29, 46} Two coal storage silos on the site hold 5,800 tons of coal each.²⁹ Approximately 1.25 million tons of coal are burned each year at the Plant.

Pulverized, powdered coal is injected into the boiler and burns at a temperature of approximately 2,800 °F (1540 °C).²⁹ Steam generated by the heated water spins the high and low pressure turbines to produce electricity. The gases produced by the combustion of coal pass through a spray dry absorber (“scrubber”) where SO₂ is removed. The Plant removes more SO₂ than is required by the regulatory agencies, thus achieving its national ranking as one of the lowest SO₂ emitting plants in the US. The coal ash is 7% fly ash and 10% bottom ash, producing approximately 87,500 tons of fly ash and 125,000 tons of bottom ash annually.

The particulate removal system at the Plant consists of a fabric filter system, referred to as a bag house. It contains 6,576 filter bags, each 34 ft (10.36 m) long, 12 in (0.31 m) in diameter, and made of Teflon® coated

fiberglass.²⁹ This particulate removal system successfully removes approximately 99.7% of the CCPs like dust, smoke, and fly ash. Those particles not removed by the bag house are emitted by the 505 ft (153.92 m) tall stack, which operates at an average opacity (visibility of the plume) of 2% which is 1/10th the maximum limit.²⁹

1.5 Conditions within the Stack

Inside the Plant's stack, the temperature varies between 200-220 °F. The volumetric flow rate within the stack is approximately 700,000 ft³ min⁻¹ (330.36 m³ s⁻¹) and the velocity is 60 ft s⁻¹ (18.29 m s⁻¹). The PM emission rate from the stack is approximately 3x10⁻³ lbs MBtu⁻¹. Approximately 8.25x10⁴ lbs yr⁻¹ (3.75x10⁴ kg yr⁻¹) of PM is released into the atmosphere.

1.6 Debate Regarding the Radioactivity and Risks of Coal Fly Ash

Review of the literature has found evidence of ²³⁸U and ²³²Th decay chains in coal.³³ There is no correlation between rank of coal and concentration of the aforementioned radionuclides. Coles³³ details the decay chains present in fly ash samples by gamma spectroscopy. The decay chain progeny producing gamma rays and the corresponding energies are listed in Table 1.5.

Various studies have been conducted to determine the relative concentration (ppm) of radioelements in coal and coal fly ash (Tables 1.6 and 1.7).

Table 1.5: Decay chain progeny present in coal, bottom ash, and fly ash³³

Decay Chain	Gamma Emitting Nuclide	Gamma Energy (keV)
²³² Th	²²⁸ Ac	338
²³² Th	²²⁸ Ac	911
²³² Th	²¹² Pb	238
²³² Th	²⁰⁸ Tl	583
²³⁸ U	²³⁴ Th	63
²³⁸ U	²²⁶ Ra	185
²³⁸ U	²¹⁴ Pb	295
²³⁸ U	²¹⁴ Pb	352
²³⁸ U	²¹⁴ Bi	609
²³⁸ U	²¹⁴ Bi	1120
²³⁸ U	²¹⁴ Bi	1764
²³⁸ U	²¹⁰ Pb	46

Table 1.6: Concentration (ppm) of elemental uranium and thorium in coal

Radioelement	Mean Concentration in Coal (ppm)	Coal Location	Coal Classification	Reference
U	0.71	Plant A	Low Sulfur	Coles et. al. ³³
	5	Plant B	Low Sulfur	Coles et. al. ³³
	1.3			Gabbard ⁵
	0.9	Plant A	Bituminous	Pacyna ⁷
	1.6	Plant B	Bituminous	Pacyna ⁷
	1.8	Plant C	Bituminous	Pacyna ⁷
	1.3	Wyodak-Anderson Study	Sub-bituminous	Stricker and Ellis ²²
	1.2	Pennsylvania	Anthracite	McBride et. al. ³⁴
	1	Appalachia	Bituminous	McBride et. al. ³⁴
	1.4	Interior (Illinois Basin)	Bituminous	McBride et. al. ³⁴
	0.7	Northern Great Plains	Sub-bituminous, Lignite	McBride et. al. ³⁴
	2.4	Gulf	Lignite	McBride et. al. ³⁴
	0.8	Rocky Mountain	Bituminous, Sub-bituminous	McBride et. al. ³⁴
	1	Alaska	Sub-bituminous	McBride et. al. ³⁴
	8.9	PRB	Sub-bituminous	USGS FS-038-02 ³⁵
	8.9	PRB	Sub-bituminous	Affolter et. al. ²³
16	Appalachia/Illinois Basin	Bituminous	USGS FS-038-02 ³⁵	
Th	1.6	Plant A	Low Sulfur	Coles et. al. ³³
	5	Plant B	Low Sulfur	Coles et. al. ³³
	3.2			Gabbard ⁵
	2.06	Plant A	Bituminous	Pacyna ⁷
	3.08	Plant B	Bituminous	Pacyna ⁷
	3.46	Plant C	Bituminous	Pacyna ⁷
	4.7	Pennsylvania	Anthracite	McBride et. al. ³⁴
	2.8	Appalachia	Bituminous	McBride et. al. ³⁴
	1.6	Interior	Bituminous	McBride et. al. ³⁴
	2.4	Northern Great Plains	Sub-bituminous, Lignite	McBride et. al. ³⁴
	3	Gulf	Lignite	McBride et. al. ³⁴
	2	Rocky Mountain	Bituminous, Sub-bituminous	McBride et. al. ³⁴
	3.1	Alaska	Sub-bituminous	McBride et. al. ³⁴
	22	PRB	Sub-bituminous	Affolter et. al. ²³

Table 1.7: Concentration (ppm) of elemental uranium and thorium in coal fly ash

Radioelement	Mean Concentration in Flyash (ppm)	Flyash Location	Coal Classification	Reference
U	5.6	ESP Plant A	Low Sulfur	Coles et. al. ³³
	8.7	Near furnace	Sub-bituminous	Affolter et. al. ²³
	8.5	Flyash collector 2	Sub-bituminous	Affolter et. al. ²³
	9	Indiana Power Plant	Sub-bituminous	USGS FS-038-02 ³⁵
	9.1	Flyash collector 1	Sub-bituminous	Affolter et. al. ²³
	9	Truck Silo	Sub-bituminous	Affolter et. al. ²³
	11	ESP Plant B	Low Sulfur	Coles et. al. ³³
Th	19	Kentucky Plant	Bituminous	USGS FS-038-02 ³⁵
	15	ESP Plant A	Low Sulfur	Coles et. al. ³³
	22	ESP Plant B	Low Sulfur	Coles et. al. ³³
	26	Flyash collector 2	Sub-bituminous	Affolter et. al. ²³
	27	Flyash collector 1	Sub-bituminous	Affolter et. al. ²³
	28	Truck Silo	Sub-bituminous	Affolter et. al. ²³
	29	Near furnace	Sub-bituminous	Affolter et. al. ²³

The concentration of metals originally in the coal, including uranium and thorium, is higher in fly ash due to the overall coal volume reduction from combustion.²⁷ Upon combustion, some radionuclides become enriched in fly ash.^{6, 12, 27, 33} The enrichment factors of these radionuclides vary in the literature from approximately 2-10. It has been concluded in many publications that the ²³⁸U decay chain shows signs of enrichment, whereas the ²³²Th decay chain does not show definitive signs of enrichment.^{12, 27, 33} The activity concentrations for ²³⁸U and ²³²Th in coal and fly ash are listed in Tables 1.8 and 1.9 below.

Table 1.8: Activity concentration in coal for ^{238}U and ^{232}Th

Radionuclide	Mean Concentration in Flyash (Bq kg ⁻¹)	Mean Concentration in Fly Ash (pCi g ⁻¹)	Flyash Location	Reference
^{238}U	70.3	1.90	Plant A	Coles et. al.
	92	2.49	Plant B	Tracy and Prantl
	129.5	3.50		Coles et. al.
	216	5.84		Weng and Chu
	200	5.41	Flue gas	UNSCEAR 1993
	700	18.92		Zeevaert et. al.
AVERAGE	234.6	6.34		
^{232}Th	58	1.57	Flue gas	Tracy and Prantl
	70	1.89		UNSCEAR 1993
	700	18.92		Zeevaert et. al.
	AVERAGE	276		7.46

Table 1.9: Activity concentration in fly ash for ^{238}U and ^{232}Th

Radionuclide	Mean Concentration in Coal (Bq kg ⁻¹)	Mean Concentration in Coal (pCi g ⁻¹)	Flyash Location	Reference
^{238}U	8.88	0.24	Plant A	Coles et. al. ³³
	12.4	0.33	Feed coal	Tracy and Prantl ¹¹
	20	0.54		UNSCEAR 1993; Beck ^{3, 36}
	29	0.78		Weng and Chu ¹²
	31.45	0.85	Plant B	Coles et. al. ³³
^{232}Th	7.5	0.20	Feed coal	Tracy and Prantl ¹¹
	10	0.27		Weng and Chu ¹²
	20	0.54		UNSCEAR 1993; Beck ^{3, 36}

Each typical plant releases approximately 5.2 tons of uranium and 12.8 tons of thorium per year.⁵ According to Beck,³ the release rate ranges of ^{238}U and ^{232}Th are 1-5 GBq GWe⁻¹ yr⁻¹ and 0.4-4 GBq GWe⁻¹ yr⁻¹ respectively. Release rates found in the literature are compiled in Table 1.10.

Table 1.10: Emission rates of ^{238}U and ^{232}Th from CFPPs

Radionuclide	Emission (GBq yr ⁻¹ GWe ⁻¹)	Emission (Ci yr ⁻¹ GWe ⁻¹)	Reference
^{238}U	0.30	0.01	McBride et. al. ³⁴
	0.30	0.01	Tadmor ¹⁰
	0.80	0.02	Corbett ³⁷
	1.0	0.03	Tadmor ¹⁰
	2.04	0.06	Aly et. al. ¹
	7.8	0.21	Tadmor ¹⁰
	18.0	0.49	Tadmor ¹⁰
^{232}Th	0.18	0.01	Tadmor ¹⁰
	0.19	0.01	McBride et. al. ³⁴
	0.40	0.01	Corbett ³⁷
	0.41	0.01	Tadmor ¹⁰
	1.26	0.03	Aly et. al. ¹
	6.70	0.18	Tadmor ¹⁰

A wide range of data has been compiled regarding dose calculations from radioactive emissions in fly ash effluent, with a range of doses. This is due to several reasons, but most important is the method of dose calculation and the concentration of radioactive contaminants in the coal used at the facility. Ranges of estimated annual dose equivalents to a maximum-exposed individual from inhalation of emissions from a coal-fired plant have been compiled by Beck. Doses ranged from 0.04 μSv (0.004 mrem) to 90 μSv (9 mrem). The maximum annual dose equivalent to the public from inhalation of resuspended materials from waste piles was estimated at most to be 5 μSv (0.5 mrem) per year.³ Dose rates found in the literature are compiled in Table 1.11.

Table 1.11: Emission rates of ^{238}U and ^{232}Th from CFPPs

Dose Rate ($\mu\text{Sv yr}^{-1} \text{GWe}^{-1}$)	Dose Rate ($\text{mrem yr}^{-1} \text{GWe}^{-1}$)	Reference
0.1	0.01	Tracy and Prantl ¹¹
0.3	0.03	NCRP 95 ³⁸ (plume)
0.7	0.07	NCRP 95 ³⁸ (resuspended materials)
19	1.9	McBride et. al. ³⁴
19	1.9	Prybutok and Gold ³⁹

There is a possibility of increased incidences of cancer due to fly ash emissions based on BEIR Reports 6 and 7.^{40, 41} As both uranium and thorium have extremely long half-lives, on the order of 10^9 years, the accumulation of these species in the biosphere is proportional to the time span the coal is burned. The accumulation of isotopes over the next 150-200 years could yield a significant radiological load on the environment.⁵ If all gaseous and particulate emissions are considered, coal fired power plants create a health risk to the population.⁶ Other health effects are possible in addition to a possible increase in radiation-induced cancers.

Some studies concluded that there are no risks and/or no measurable radioactivity in coal fly ash.²⁷ Others conclude that, while there is no measurable activity,¹¹ there is still a possibility of risk to humans and the environment from radionuclides present in the fly ash.^{1, 11} Most studies agree that radioactivity is present in fly ash. Although the amount of activity present is quite small, there is a risk to humans and the environment^{2-10, 12} based upon the concept of the linear, no-threshold model.⁴¹

1.7 Respirable Particulate Matter

Inhalability is defined as the fraction of suspended material in ambient air that enters the nose or mouth as a volume of air is inhaled.⁴² If particles do not enter the nose or mouth, they are unavailable for inhalation and can cause an overestimate to the dose if included in the dose estimation. A healthy adult processes 10-25 m³ of air per day and has an alveolar surface area of 75 m².⁴³ For an individual at rest, approximately 0.5 L of air is inhaled and exhaled with each breath.⁴³ This is known as the tidal volume and can be three times higher for an individual under exertion. The normal breathing rate of a healthy adult is approximately 12 breaths per minute with a flow rate of approximately 1 L s⁻¹.⁴³

After particles have been inhaled, they deposit by three basic mechanisms depending upon the size of their aerodynamic diameter: inertial impaction, sedimentation, and diffusion. Particles that deposit via inertial impaction have enough inertial force that they do not follow the exact air stream lines within the airway and thus may impact upon the walls.^{42, 43} This mechanism predominates for particles larger than 1 µm in diameter.⁴² Sedimentation occurs for particles which have enough mass to be largely influenced by gravity and have increased settling velocities.⁴³ These particles (those larger than 0.5 µm in diameter) settle onto the lower surfaces of the airway.⁴² For smaller particles, Brownian motion due to collisions with air molecules may cause particles smaller than 0.5 µm to travel out of the stream

line and deposit onto the walls of the airway. This is known as diffusion and predominates for particles smaller than 0.5 μm in diameter.

Particulate matter that is able to deposit in the pulmonary⁴² or the alveolar-interstitial region^{43, 44} region of the lung is considered to be respirable. The alveolar region is of particular importance due to its physiological purpose: gas exchange. If radioactive particles reach the alveolar region of the lung, they are exchanged into the blood stream for circulation throughout the body. Particles that are larger than 10 μm in diameter do not typically reach the alveolar region and particles 2-10 μm in diameter reach this region in attenuated numbers.⁴³ During mouth breathing, the particle sizes most likely to deposit in the alveolar region are 3-4 μm in diameter.^{42, 43} The particles most likely to deposit in the alveolar region during nose breathing are those that are 2 μm in diameter.

Chapter 2: Materials and Methods

2.1 Sampling for Radioactivity

2.1.1 *Fly Ash Grab Sampling and Gamma Spectroscopy*

A grab sample of fly ash was taken from the fabric filter (bag house) at the Plant. This step was necessary to understand the radionuclides present in the fly ash. The sample was placed in a sealed marinelli beaker for 30 days to allow the radon and thoron daughters to equilibrate.³³ Gamma spectroscopy was performed using an Canberra HPGe detector (model GC 1418, Meriden, CT) for a 24 hour period (operating voltage, 4500 V; amplifier (Canberra 2026, Meriden, CT) settings: course gain, 10 and fine gain 12.2; ADC (Canberra MP2-1U, Meriden, CT), 4096 channels). Gamma spectroscopy was used to identify, qualitatively, whether the ^{238}U and ^{232}Th decay chains (figs. 2.1-2) were present in the sample by identifying the respective gamma emitting daughters.

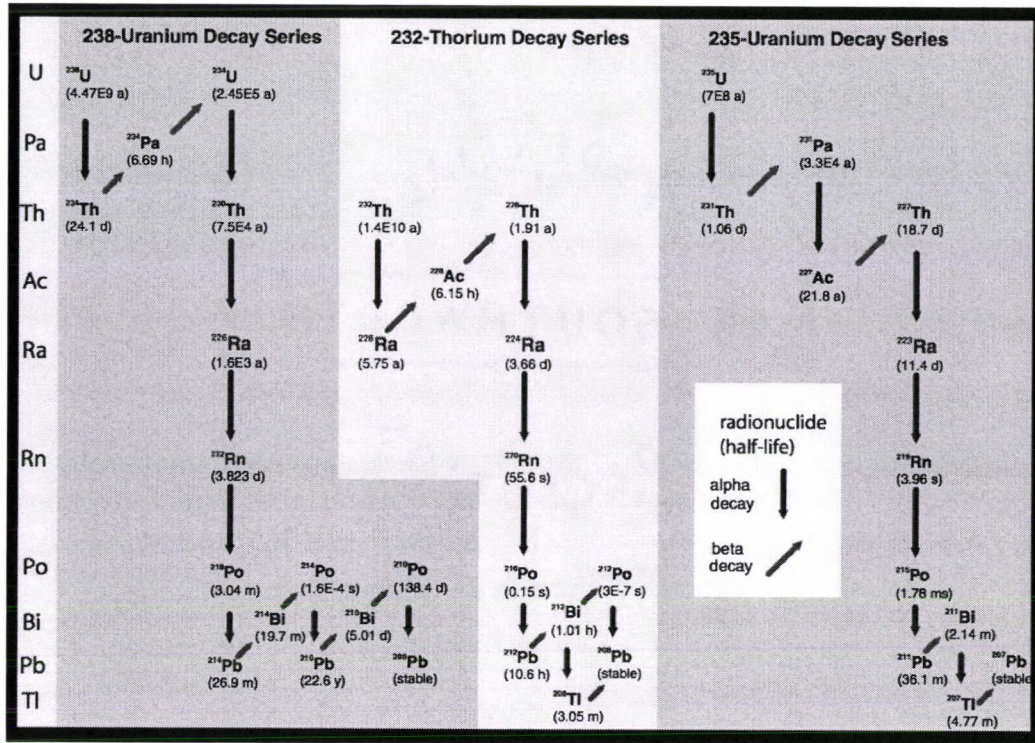


Figure 2.1: Decay chains provided by the USGS⁴⁷

2.1.2 Determination of Limit of Detection for Gross Alpha and Beta Counting

The limit of detection used for gross alpha and beta counting is defined in this instance as the amount of mass with a count rate that yields the minimum count rate above background. This was done in preparation for size distribution determination. Twenty-three aliquots of fly ash were weighed using a Fisher Scientific A-160 (Pittsburg, PN) balance in 10^{-3} g – 10^1 g magnitude increments (masses listed in Tables 3.2-3.3). Samples were counted with a Tennelec LB5100 (Oak Ridge, TN) thin-window (Mylar, $500 \mu\text{g cm}^{-2}$)⁴⁸, gas-flow proportional counter using P-10 gas, for 40 minutes, at the operating voltage of 1400 V (Tennelec TC951, Oak Ridge, TN), a Tennelec (Oak Ridge, TN) low/wide beta amplifier/discriminator settings (TC264A; gain, 64; discriminator, 9), and a Tennelec (Oak Ridge, TN) low/wide beta

amplifier/single channel analyzer settings (TC265A; gain, 16; alpha, 200; alpha + beta, 28).

The data were analyzed by calculating the count rate and standard deviations for each of the aliquots. Those masses that contained a net count rate above decision level were determined using a t-test and the International Standards Organization's (ISO) decision level calculation.⁴⁹ Samples with a t-statistic greater than 1.645 (95 percent confidence limit with a one-tailed t-test) and net count rates greater than the corresponding decision level were determined to contain statistically significant count rates above background levels.^{49, 50}

$$t_{calc} = \frac{R_g - R_b}{\sqrt{\frac{R_g}{t_g} + \frac{R_b}{t_b}}} = \frac{R_n}{s_n} \quad (\text{Eqn 2.1})$$

Where:

- R_g denotes gross count rate
- R_b denotes blank count rate
- R_n denotes net count rate
- t_g denotes sample count time
- t_b denotes blank count time
- s_n denotes standard deviation of the net count rate

$$DL_{ISO}(R_n, \alpha) = R_n^* = \frac{k_{1-\alpha}^2}{2t_0} \left(1 + \sqrt{1 + \frac{4R_b t_b}{k_{1-\alpha}^2} \left(1 + \frac{t_b}{t_g} \right)} \right) \quad (\text{Eqn 2.2})$$

Where:

- R denotes count rate
- t denotes time
- b denotes blank
- g denotes sample
- n denotes net
- $*$ denotes a statistic
- α denotes the 'false positive,' type I error probability
- $k_{1-\alpha}$ denotes standard normal deviate $1-\alpha$, $k_{0.95} \sim 1.65$

2.2 Study Design

2.2.1 Fly Ash Size Fractionation

The fly ash sample was sized at the Colorado State University's Soil-Water-Plant Testing Laboratory. Sizing was accomplished using sieving and pipetting techniques. Particle sieving was used to separate the sample into physical diameters that were coarser than 20 μm . Shaking the sample in meshes that decrease in size ensured that the particles smaller than 20 μm could be further analyzed for size using the pipetting technique.

A pipetting technique was used to determine the number of particles with diameters from 1-20 μm . A pipetting technique utilizes the principles of sedimentation in a liquid medium (aqueous sodium hexametaphosphate) to ascertain particle sizes. The Stokes' equation was used for the relationship between size of a spherical particle and its settling velocity.⁵¹ Small spherical particles of density ρ_p and diameter d are known to settle through a liquid of density ρ_L and viscosity η , where g is acceleration due to gravity.⁵¹

$$V_{TS} = \frac{d^2 g (\rho_p - \rho_L)}{18\eta} \quad (\text{Eqn 2.3})$$

Separation of each fraction by sedimentation was accomplished by homogenizing a sample suspension and decanting that which remains above the line, $z = -h$, after time, t .⁵¹

$$t = \frac{18\eta h}{d^2 g (\rho_p - \rho_L)} \quad (\text{Eqn 2.4})$$

The larger the particle diameter, the faster the particle falls in the solution. Those particles that settled in depth (h) at a given sedimentation time (t) for a

specific aerodynamic diameter are collected by a pipetted volume in that depth. The particles larger than d in the Stokes' equation, are removed by the pipette, and all particles smaller than that size remain suspended in the liquid.⁵¹ The volume of liquid with suspended PM at depth, h , that was screened by the process of sedimentation, was removed and weighed. The weight (w) of particles and solution present in that volume at the sedimentation time (t) was divided by the weight (w_0) of all particles present in the liquid medium initially. This ratio is equal to the percentage of particles by weight smaller than the diameter, d .⁵¹

Mass was collected into size fractions (>20 μm , 14 μm , 10 μm , 5 μm , 3 μm , and 1 μm) for counting purposes and radiochemical analysis. These masses of given size fractions were used to determine the mass median aerodynamic diameter (MMAD) by using log probability paper and the "eyeball regression" technique as described in DiNardi⁵², adopted by Industrial Hygienists.⁵² The activity concentrations for ^{238}U and ^{232}Th were used to find an activity median aerodynamic diameter (AMAD), using the same technique described for the MMAD.

2.2.2 Gross Alpha and Beta Counting

The Tennelec LB5100 Low Background Counting System was used to detect low-level alpha and beta radiation. It utilizes a gas-flow proportional detector surrounded by four inches of low background lead and oxygen-free high-conductivity copper for shielding backscatter photons.⁴⁸ It has an

automated sample changer assembly for counting multiple samples. The performance of this system depends on several factors: sample rate, background rate, and the electronics. Sample counting rate depends on the absorption of the radiation's energy through the Mylar window, the geometric relationship between the sample and the detector, the detection probability, the detector's area, and the scattering effects.⁴⁸ As sources emit radiation isotropically, it is ideal for a detector to completely surround the source (4π geometry). However, this detector provides 2π geometry as a compromise between cost and effectiveness. This detector has a sample holder with a diameter slightly smaller than the detector window diameter, which reduces the air gap between the sample tray and the detector window.⁴⁸

After the samples were massed (as described in section 2.1b) the LB5100 was used to count the samples in each of the five size fractions. The LB5100 was used to count all the samples for gross alpha and beta radiation. The samples were counted with a background count before and after each sample. Each sample was counted for 60 minutes and alpha and beta counts were recorded.

2.2.3 Radiochemical Analysis

Radiochemical analysis was performed by a local analytical laboratory. An explanation of their operating procedures and radiochemical theory is described in this section. In order to quantify and qualify the ^{238}U and ^{232}Th (actinides) present in fly ash, radiochemical analysis was performed. This

was necessary to determine activity concentrations of the aforementioned isotopes for dose calculation. Tracers were added, ^{232}U and ^{229}Th , for the radioisotopes of interest (U and Th respectively) as a marker or tag for labeling and identification. As these tracers are strong gamma emitters, this allows their respective “tagged” species to be easily detected during the analytical process with survey equipment (Geiger-Mueller counters or NaI detectors). Dissolution of the sample was accomplished with 16 M nitric acid (HNO_3), 29 M hydrochloric (HCl), and 12 M hydrofluoric acid (HF).⁵³ A hydroxide co-precipitation was necessary to pre-concentrate the actinides and remove components that do not form insoluble hydroxides.⁵³ The precipitate resulting from the hydroxide co-precipitation was dissolved in HCl. Impurities from this solution were removed using an ion-exchange column.

The ion-exchange column had an anion-exchange resin that was equilibrated in 9 M HCl.⁵⁴ This molarity of HCl in the anion exchange resin allows for adsorption of U, while the other elements in the sample, including Th, passed through the column and were collected for further analysis. The U was stripped by washing the resin with 0.5 M HCl as this molarity of HCl does not allow for adsorption of U on the anion exchange resin.⁵⁴ The U and Th were co-precipitated with lanthanum fluoride and were mounted for alpha spectroscopy.

Once the laboratory separated the radioactive species of interest, alpha spectroscopy was performed to determine the activity concentration of

^{238}U and ^{232}Th in fly ash. The laboratory's alpha spectroscopy operating procedures and the detector theory is described below.

Alpha particles create free electrons and holes within semiconductor material. As the free electrons pass to the valence band and the holes pass to the conducting band of the detector, pulses are created.⁵⁵ The energy deposited by the alpha particles in the silicon wafer (semiconductor) of the Octet PC alpha spectrometer by EG&G Ortec (Oak Ridge, TN; operating voltage, 50 V) creates a pulse for each interaction. The pulse-height created is proportional to the energy of the alpha particle. As air is a very successful attenuator for alpha particle energy, application of a vacuum minimizes the amount of alpha energy lost before it reaches the detector. The data were collected and processed using a computer software package, AlphaVision 32 ®, v5.3 (Ortec, Oak Ridge, TN).⁵⁶

2.2.4 *Determination of Whole Body Dose from Inhalation Exposure*

The AMAD of the fly ash was calculated once the activity concentrations of ^{238}U and ^{232}Th in the fly ash were determined. The cumulative activity concentration was found using the same technique as described for the MMAD in section 2.2.1. The occupational committed effective dose equivalent (CEDE) was calculated using the annual limit on intake (ALI) for ^{238}U and ^{232}Th .

The ALI is the amount of activity necessary for an individual to receive the annual CEDE of 5 rem for the entire body (SALI) or the committed dose

equivalent of 50 rem to any organ (NALI).¹⁴ The inhalation ALIs are listed in 10 CFR 20 Appendix B for each radionuclide, providing the aerosol has an AMAD of 1 μm and has a biological half life falling into one of three classes: days, weeks, years (D, W, Y) for ICRP 30 and fast, medium, slow (F, M, S) for ICRP 60. In order to use the correct ALI, it is necessary to understand the solubility of the particles inhaled. Radioactive aerosols have a class D/F ALI when the chemical form is highly soluble, while those that have a class Y/S ALI are highly insoluble.

As the AMAD of a particle changes, deposition fraction in the nasopharyngeal (NP), tracheobronchial (TB), and pulmonary (P) regions change. Therefore, the ALI for radioactive aerosols with AMAD not equal to 1 μm must be corrected or adjusted to account for the different deposition distribution within the airway. The ALI correction for the i th particle size is illustrated in equation 2.5.⁵⁰

$$H_{50}(i) = H_{50}(1\mu\text{m}) \left[f_{NP} \left(\frac{D_{NP}(i)}{D_{NP}(1\mu\text{m})} \right) + f_{TB} \left(\frac{D_{TB}(i)}{D_{TB}(1\mu\text{m})} \right) + f_P \left(\frac{D_P(i)}{D_P(1\mu\text{m})} \right) \right] \quad (\text{Eqn 2.5})$$

Where:

- H_{50} denotes committed effective dose equivalents from the 1 μm and i th μm AMAD particles
- f_{NP}, f_{TB}, f_P denotes fractions of CEDE due to deposition in the NP, TB, and P regions from ICRP 30
- D_{NP}, D_{TB}, D_P denotes deposition fractions in the respiratory compartments for a given particle size

Dose to the public was calculated for the nuclides of interest using the ALIs found in 10 CFR 20 Appendix B where the CEDE is 100 mrem per

year.^{14, 57} The occupational values and effluent concentrations for ²³⁸U and ²³²Th from 10 CFR 20 Appendix B are provided in Tables 2.2-2.3 below.

Table 2.2: Occupational values and effluent concentrations for ²³⁸U

Uranium-238

Atomic No.	Radionuclide	Class	Table 1 Occupational Values			Table 2 Effluent Concentrations		Table 3 Releases to Sewers
			Col. 1	Col. 2	Col. 3	Col. 1	Col. 2	Monthly Average Concentration (μCi/ml)
			Oral Ingestion ALI (μCi)	Inhalation		Air (μCi/ml)	Water (μCi/ml)	
				ALI (μCi)	DAC (μCi/ml)			
92	Uranium-238 ³	D, see ²³⁰ U	1E+1 Bone Surf	1E+0 Bone Surf	6E-10	-	-	-
			(2E+1)	(2E+0)	-	3E-12	3E-7	3E-6
		W, see ²³⁰ U	-	8E-1	3E-10	1E-12	-	-
		Y, see ²³⁰ U	-	4E-2	2E-11	6E-14	-	-

Table 2.3: Occupational values and effluent concentrations for ²³²Th

Thorium-232

Atomic No.	Radionuclide	Class	Table 1 Occupational Values			Table 2 Effluent Concentrations		Table 3 Releases to Sewers
			Col. 1	Col. 2	Col. 3	Col. 1	Col. 2	Monthly Average Concentration (μCi/ml)
			Oral Ingestion ALI (μCi)	Inhalation		Air (μCi/ml)	Water (μCi/ml)	
				ALI (μCi)	DAC (μCi/ml)			
90	Thorium-232	W, see ²²⁶ Th	7E-1 Bone Surf	1E-3 Bone Surf	5E-13	-	-	-
			(2E+0)	(3E-3)	-	4E-15	3E-8	3E-7
		Y, see ²²⁶ Th	-	3E-3 Bone Surf	1E-12	-	-	-
			-	(4E-3)	-	6E-15	-	-

The amount of inhaled PM mass necessary to meet the CEDE for workers (5 rem) and the whole body dose limit for the public (100 mrem) was calculated using the relationship between activity concentration (Bq g⁻¹) and size (μm) of the respirable portion of the fly ash and the ALI for ²³⁸U and ²³²Th.

Chapter 3: Data and Analysis

3.1 Gamma Spectroscopy of Fly Ash

A sample of fly ash, weighing 17.29 g, was analyzed using gamma spectroscopy. The sample was counted for 24 hours with a 1 hour blank count prior. Upon completion of the count, the ambient background and the spectrum were analyzed using Genie 2000 software. Background was found to be negligible as only two unidentified peaks (352.73 and 609.54 keV) were found. Since the blank was a sealed empty Marinelli beaker, these two unidentified peaks were most likely the radon daughters ^{214}Bi (609.31 keV, yield 46.30%) and ^{214}Pb (351.92 keV, yield 37.20%) found in ambient air that were trapped in the empty beaker. The identification of each nuclide in the sample and their representative decay chain are listed in Table 3.1. These results provide strong evidence that both ^{238}U and ^{232}Th decay chains are present in fly ash material. There is also some evidence of the ^{235}U decay chain in fly ash.

Table 3.1: Peak identification output from spectroscopy software

Identification	Identification Confidence	Energy (keV)	Energy Detected (keV)	Yield (%)	Decay Chain
^{212}Bi	0.724	39.86	39.86	1.1	^{232}Th
		727.17	727.17	11.8	
		785.42	785.42	2	
^{212}Pb	0.933	1620.56	1619.06	2.75	^{232}Th
		74.81	74.81	9.6	
		77.11	77.11	17.5	
		87.2	87.2	6.3	
		89.8	89.8	1.75	
		115.19	115.19	0.6	
		238.63	238.63	44.6	
^{214}Bi	0.475	300.09	300.09	3.41	^{238}U
		609.31	609.31	46.3	
		768.36	768.36	5.04	
		806.17	806.17	1.23	
		934.06	934.06	3.21	
		1120.29	1120.29	15.1	
		115.19	115.19	1.69	
		1238.11	1237	5.94	
		1280.96	1279.76	1.47	
		1377	1376.3	4.11	
		1385.31	1383.94	0.78	
		1401.5	1400.09	1.39	
		1407.98	1406.53	2.48	
		1509.19	1507.57	2.19	
		1661.28	1659.59	1.15	
		1729.6	1727.58	3.05	
		1764.49	1762.49	15.8	
1847.44	1845.17	2.12			
^{214}Pb	0.955	2118.54	n/d	1.21	^{238}U
		74.81	74.81	6.33	
		77.11	77.11	10.7	
		87.2	87.2	3.7	
		89.8	89.8	1.03	
		241.98	241.98	7.49	
		295.21	295.21	19.2	
		351.92	351.92	37.2	
^{219}Rn	0.965	785.91	785.91	1.1	^{235}U
		271.23	271.23	9.9	
^{228}Ac	0.576	401.78	401.78	6.6	^{232}Th
		89.95	89.95	2.1	
		93.35	93.35	3.5	
		129.08	129.08	2.8	
		209.28	209.28	4.4	
		270.23	270.23	3.6	
		327.64	327.64	3.2	
338.32	338.32	11.4			

		409.51	409.51	2.13	
		463	463	4.4	
		794.7	794.7	4.6	
		911.6	910.6	27.7	
		964.6	964.6	5.2	
		969.11	969.11	16.6	
		1587.9	1590.62	3.71	
²³¹ Th	0.946	26.64	n/d	18.7	²³⁵ U
		84.21	84.21	8	
		89.95	89.95	1.25	
^{234m} Pa	0.951	1001.03	1001.03	0.59	²³⁸ U
²³⁵ U	0.675	89.96	89.96	1.5	²³⁵ U
		93.35	93.35	2.5	
		105	106.23	1	
		109.14	109.14	1.5	
		143.76	143.76	10.5	
		163.35	n/d	4.7	
		185.71	185.71	54	
		202.12	n/d	1	
		205.31	n/d	4.7	
²²⁶ Ra		186	185.71	3.59	²³⁸ U

3.2 Gross Alpha and Beta Limit of Detection for Fly Ash Mass and Calibration Curves

Count data from the massed aliquots were collected and plotted as count rate (cps) vs. mass (mg) with log transformation on both axes (Figure 3.1-3.2). The limit of detection was determined to be 44 mg for gross alpha counting and 119 mg for gross beta counting based the decision level and t-test results (Table 3.2-3.3).

Table 3.2: Detectable count rate above background for alpha particles

Mass (mg)	Net count rate (cps)	SD	t-calc	>1.645?	Detection Level	net cpm above DL?
1.4	0.001	0.002	0.53	n	0.0030	n
33.2	0.003	0.002	1.41	n	0.0030	n
4.1	0.004	0.002	1.96	y	0.0030	y
5.6	0.005	0.002	2.29	y	0.0030	y
7.2	0.001	0.002	0.77	n	0.0030	n
11	0.000	0.001	0.00	n	0.0030	n
13.2	0.002	0.002	1.00	n	0.0030	n
19.6	0.000	0.001	-0.30	n	0.0030	n
44	0.008	0.002	3.79	y	0.0025	y
63.1	0.003	0.002	1.77	y	0.0025	y
57.2	0.004	0.002	2.34	y	0.0025	y
118.9	0.012	0.002	4.78	y	0.0025	y
152.2	0.013	0.003	5.08	y	0.0025	y
142.5	0.009	0.002	4.03	y	0.0025	y
650.5	0.011	0.002	4.68	y	0.0025	y
525.9	0.016	0.003	5.71	y	0.0025	y
530.8	0.011	0.002	4.58	y	0.0025	y
1039.6	0.018	0.003	5.89	y	0.0029	y
1119.5	0.012	0.003	4.64	y	0.0029	y
1452.2	0.011	0.003	4.43	y	0.0029	y
2443	0.016	0.003	5.56	y	0.0029	y
3379	0.023	0.003	6.73	y	0.0029	y
5115	0.021	0.003	6.44	y	0.0029	y

Table 3.3: Detectable count rate above background for beta particles

Mass (mg)	Net count rate (cps)	SD	t-calc	>1.645?	Detection Level	Net cps above DL?
1.4	0.005	0.017	0.29	n	0.029	n
3.2	0.010	0.017	0.56	n	0.029	n
4.1	0.014	0.017	0.79	n	0.029	n
5.6	0.027	0.017	1.55	n	0.029	n
7.2	0.013	0.017	0.72	n	0.029	n
11	0.004	0.017	0.24	n	0.029	n
13.2	0.013	0.017	0.75	n	0.029	n
19.6	0.010	0.017	0.60	n	0.029	n
44	0.029	0.017	1.69	y	0.029	y
63.1	0.014	0.017	0.84	n	0.029	n
57.2	-0.002	0.017	-0.13	n	0.029	n
118.9	0.047	0.018	2.69	y	0.029	y
152.2	0.038	0.017	2.18	y	0.029	y
142.5	0.047	0.018	2.67	y	0.029	y
650.5	0.142	0.019	7.60	y	0.029	y
525.9	0.091	0.018	5.03	y	0.029	y
530.8	0.124	0.018	6.69	y	0.029	y
1039.6	0.179	0.019	9.42	y	0.028	y
1119.5	0.204	0.019	10.62	y	0.028	y
1452.2	0.205	0.019	10.64	y	0.028	y
2443	0.309	0.020	15.17	y	0.028	y
3379	0.354	0.021	17.04	y	0.028	y
5115	0.444	0.022	20.50	y	0.028	y

In the event that mass losses occurred during the analysis process, it was necessary that at least 1 gram of fly ash material per size fraction be obtained. This was expressed to the CSU Soil-Water-Plant Testing laboratory prior to the implementation of the pipetting separation technique.

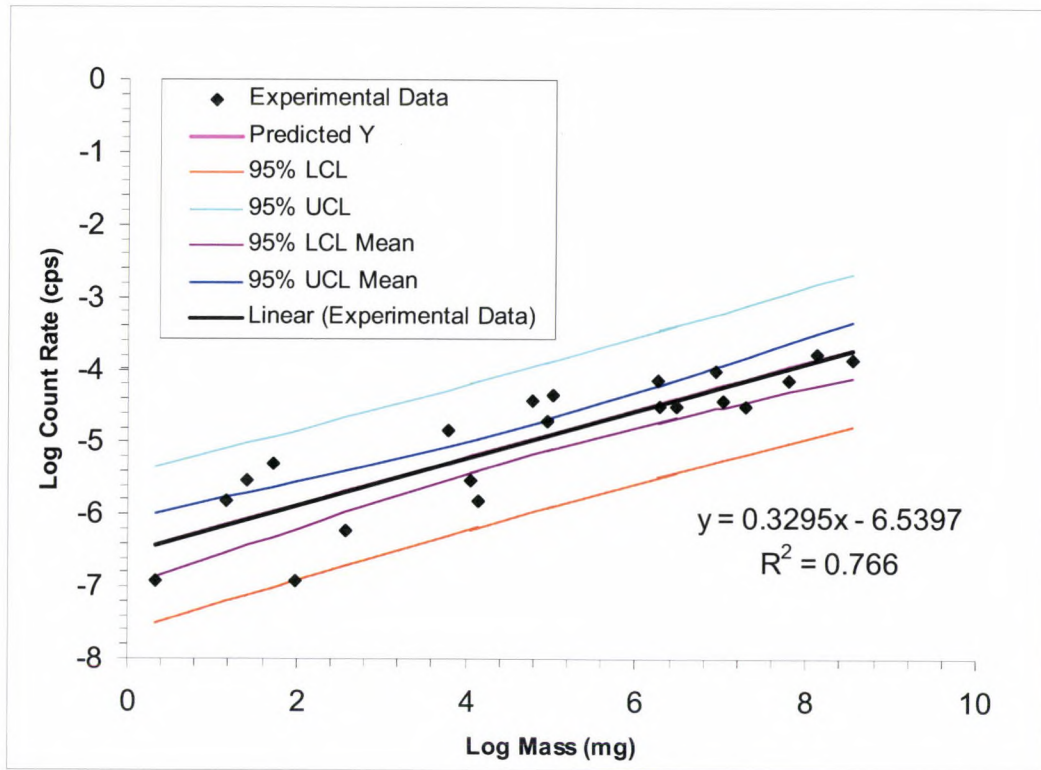


Fig. 3.1: Relationship between gross alpha net count rate and mass with a log transformation

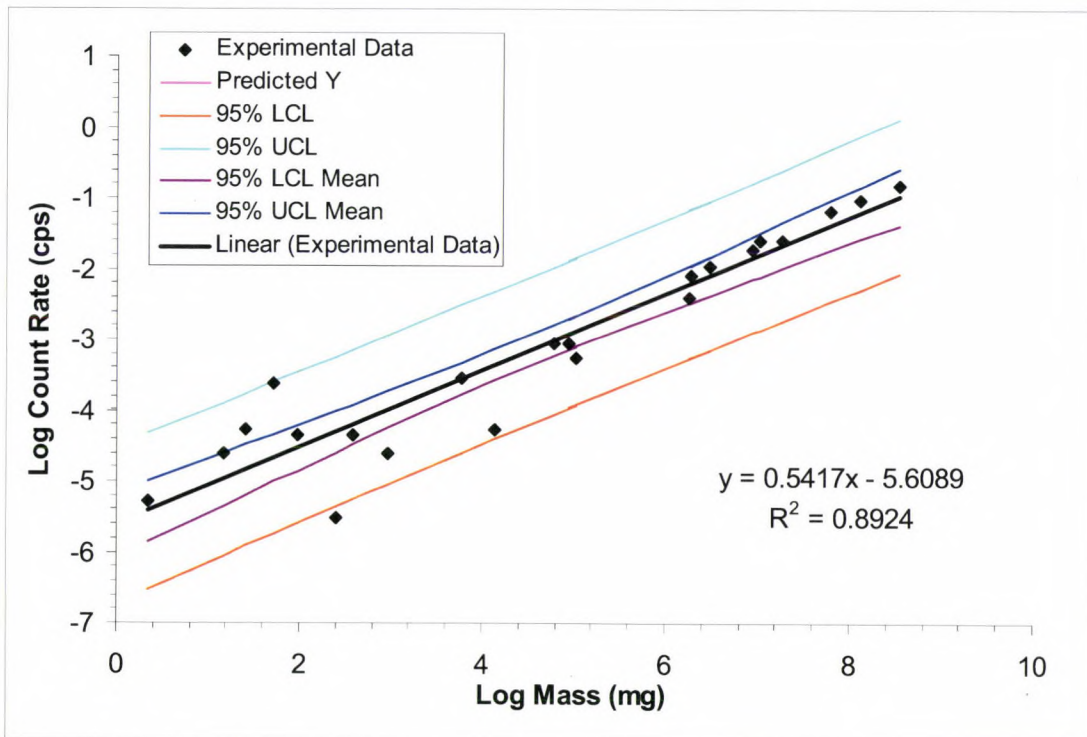


Fig. 3.2: Relationship between gross beta net count rate and mass with a log transformation

3.3 Count Rate vs. Sample Mass Relationship and Statistics

3.3.1 Gross Alpha Count Rate vs. Sample Mass Relationship

A linear regression was applied to a log transformation of sample mass vs. gross alpha count rate. However, tests for normality indicated normality for a linear transformation and non-normality for a log transformation, while q-q plots and histograms for each transformation indicated non-normality for both (Appendix C).

3.3.1a Linear Transformation

The linear transformation for gross alpha count rate vs. sample mass data was plotted and evaluated (Figure 3.3).

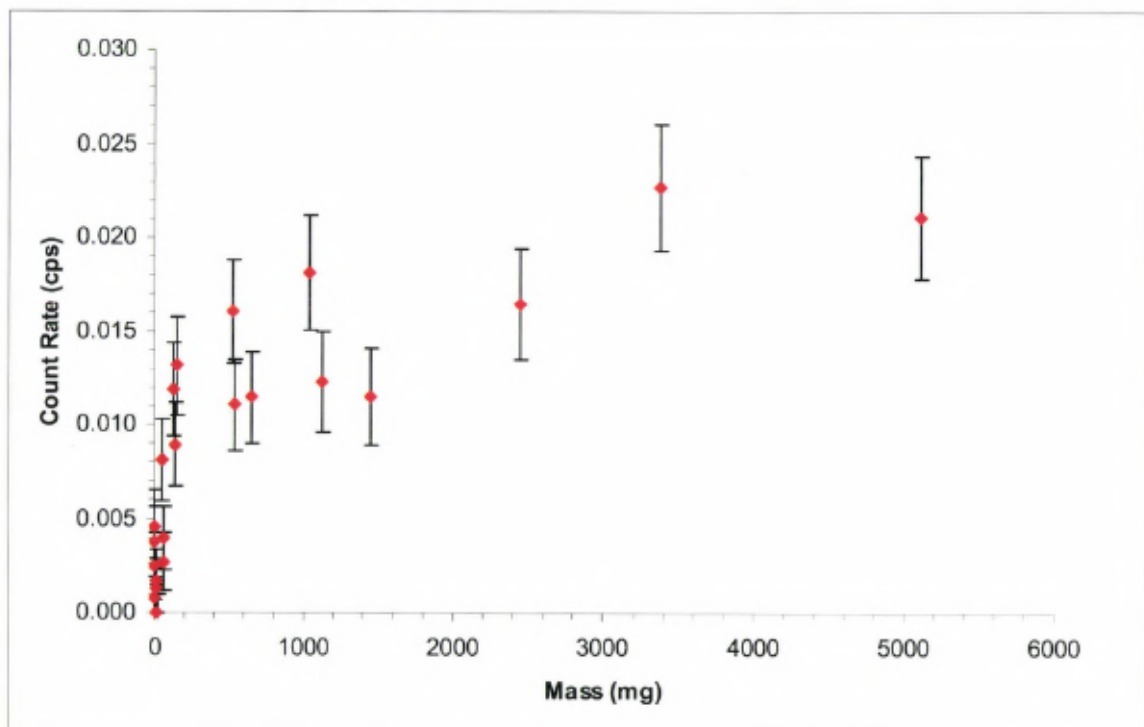


Figure 3.3: Alpha Count Rate vs. Sample Mass, linear transformation with error bars representing one standard deviation

There was a sharp increase in the alpha count rate for aliquots with masses of fly ash less than 100 mg. Those aliquots greater than 100 mg in mass gradually increase in alpha count rate and approach an asymptote. Using iterative techniques for non linear regression in SAS statistical software, an asymptote of approximately 0.0156 cps was found (Appendix E and Figure 4.2).

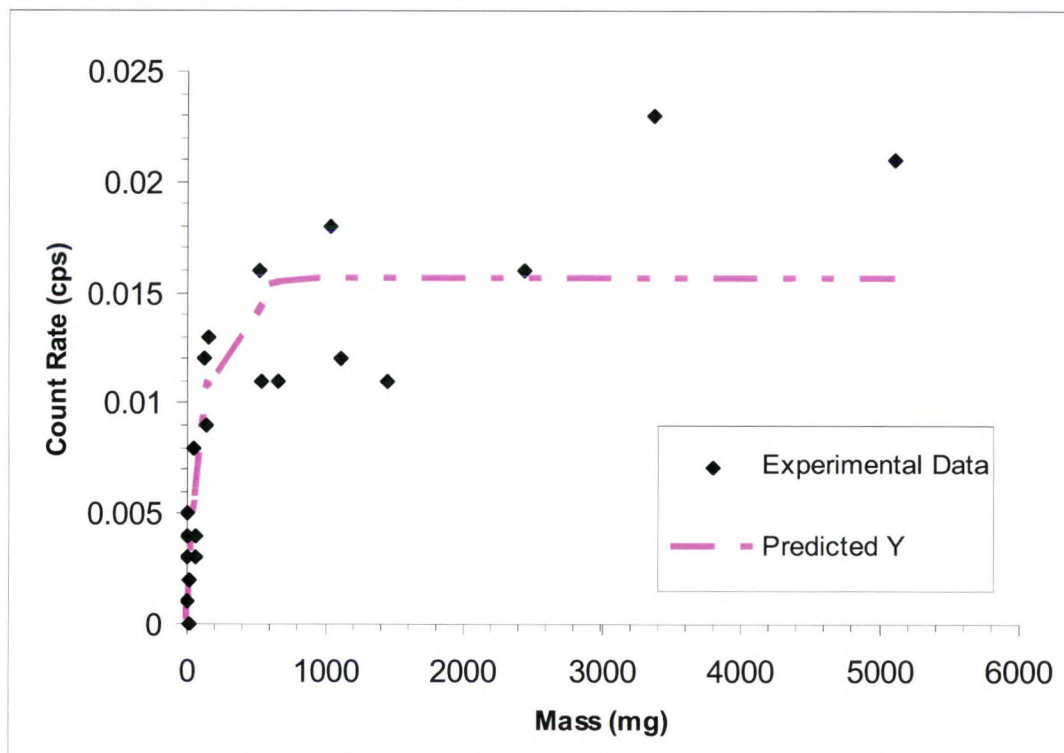


Figure 3.4: Non-linear regression of alpha count rate vs. mass data, linear transformation
The non-linear regression in Figure 4.2 may not be an accurate model due to the unavailability of data at larger masses, poor residual plots (Figure 3.5), and evidence of autocorrelation (Appendix E).

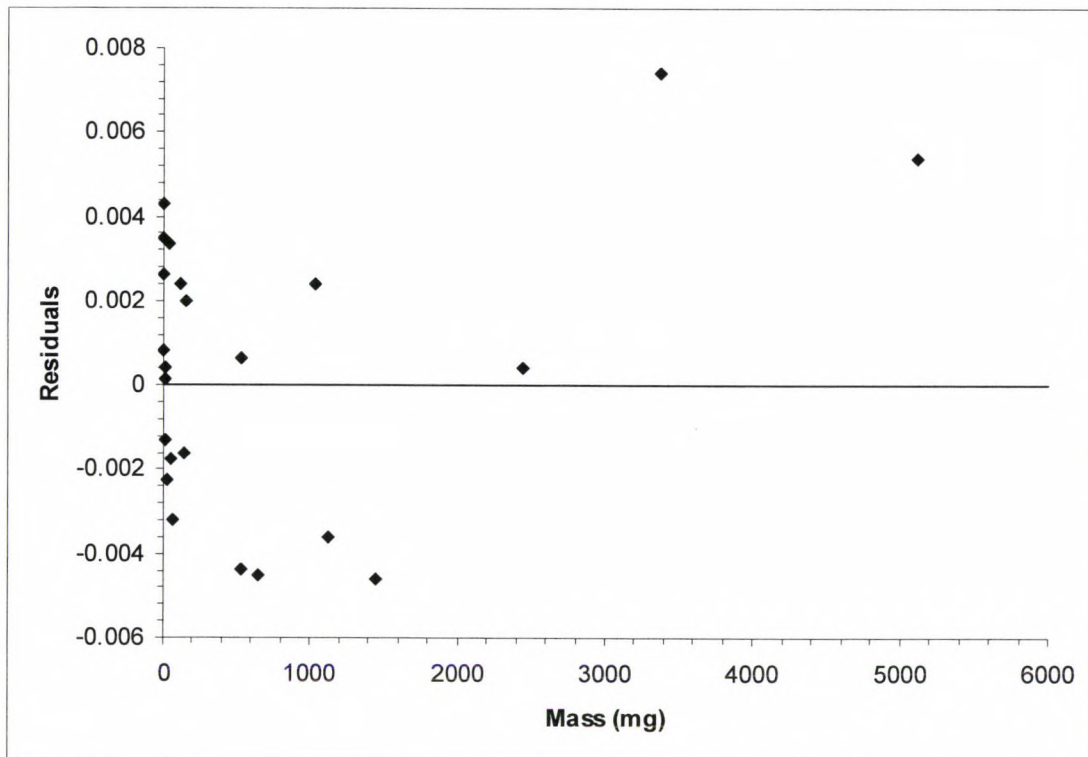


Figure 3.5: Residual plot for alpha count rate vs. mass data, linear transformation

3.3.1b Logarithmic Transformation

A logarithmic transformation with a linear regression was used to analyze the alpha count rate vs. fly ash mass data and plotted with all data points between the 95% confidence intervals of the regression line (Figure 3.1). There is an increasing relationship between count rate and mass with more variability in the count rate at lower masses than for higher masses (Figure 3.1). This can be also seen in the residual plot (Figure 3.6).

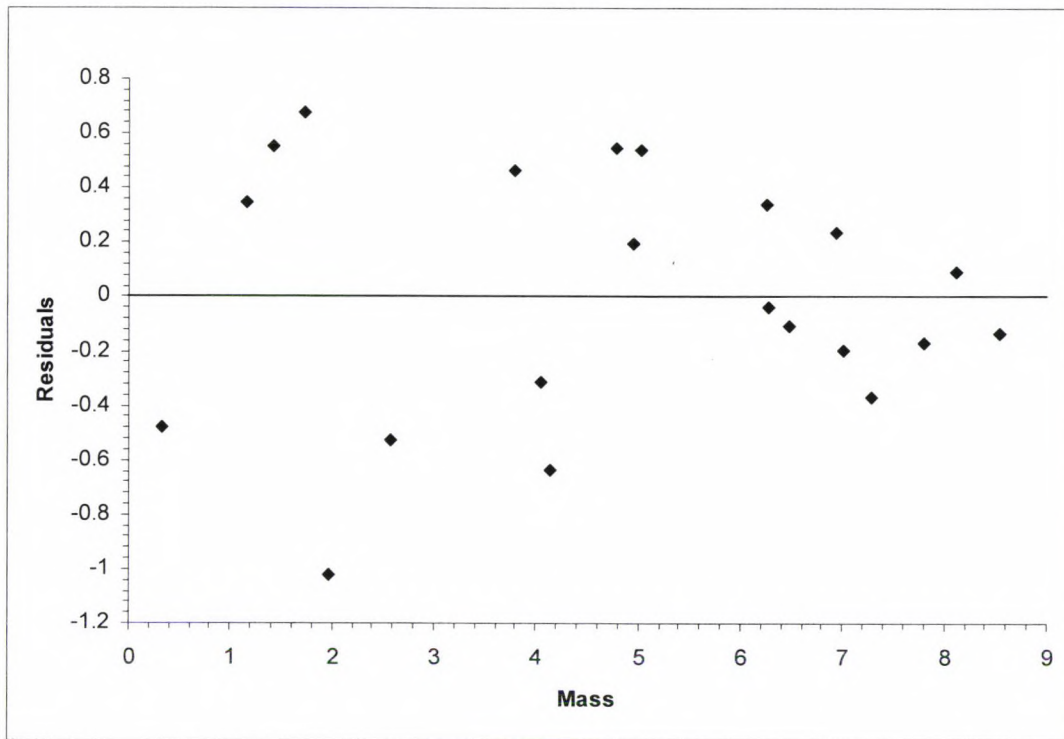


Figure 3.6: Residual plot for alpha count rate vs. mass data, log transformation

Absence of autocorrelation is essential for a linear regression model to be a reasonable representation of the data.⁵⁸ There is absence of autocorrelation in the logarithmic transformation of the gross alpha count rate vs. fly ash mass data (Appendix E). The linear transformation of the same data has evidence of autocorrelation (section 3.3.1a). Therefore, the logarithmic transformation with linear regression was selected as the best model for these data.

3.3.2 Gross Beta Count Rate vs. Sample Mass Relationship

The gross beta count rate data were log transformed. A linear regression was utilized to describe the relationship between the log transformed gross beta count rate and fly ash mass. Tests for normality

indicated non-normality for a linear transformation and normality for a log transformation (Appendix D). The q-q plot and histogram for the linear data indicate non-normality (Appendix D). However, both plots indicate the possibility of a bimodal distribution (Appendix D).

A logarithmic transformation with a linear regression was applied to the data and plotted with only 1 data point outside the 95% confidence intervals of the regression line out of 23 data points (Figure 3.2). One point outside the 95% confidence interval is acceptable since at 95% confidence level, 1.15 data points are expected to fall outside the confidence interval due to random chance.

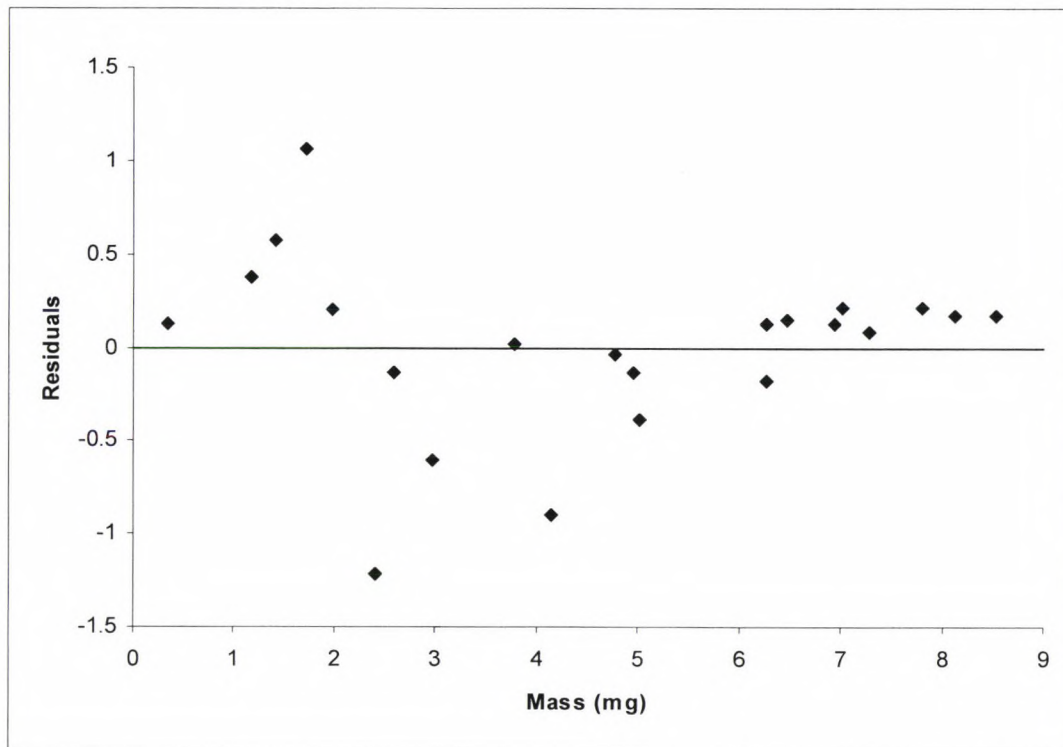


Figure 3.7: Residual plot for beta count rate vs. mass data, log transformation

3.4 Fly Ash Particle Size Distribution

Particle sizing of the fabric filter fly ash material revealed that 13.78% of the mass was associated with particles 20 μm and smaller, while 86.22% of the mass was associated with particles greater than 20 μm (Table 3.2).

Table 3.2: Particle size distribution of fly ash samples

Particle Size Upper Limit (μm)	Distribution (wt %)
>20	86.22
20	3.56
14	2.87
10	2.49
5	2.68
3	1.26
1	0.92

The size distribution is not the same as the size distribution of the PM within in the stack, as a fabric filter system is designed to remove large PM in the flue gas before it exits through the stack. Thoracic particles are those reaching the TB region during inhalation (10-20 μm and smaller in size).⁴³ Fabric filter particulate removal systems are more efficient for particles larger than 20 μm .⁵⁹ Particle size categories were truncated at 20 μm to represent the size distribution of fly ash within the stack. The corrected MMAD was determined to be 7.4 μm with a geometric standard deviation (GSD) of 2.5 using the method described in section 2.2a.

3.5 Gross Alpha and Beta Activity Concentration vs. Particle Size

Aliquots of PM in each size range were massed using the method described in 2.1b. Count data from the massed aliquots were collected and

plotted as activity concentration (pCi g^{-1}) vs. size (μm) (Figure 3.8-3.9). For both alpha and beta counting, activity concentration increased with increasing particle size. Both a linear and non linear regressions were fitted to the data to ascertain the best fit model. The data represent a non-linear trend.

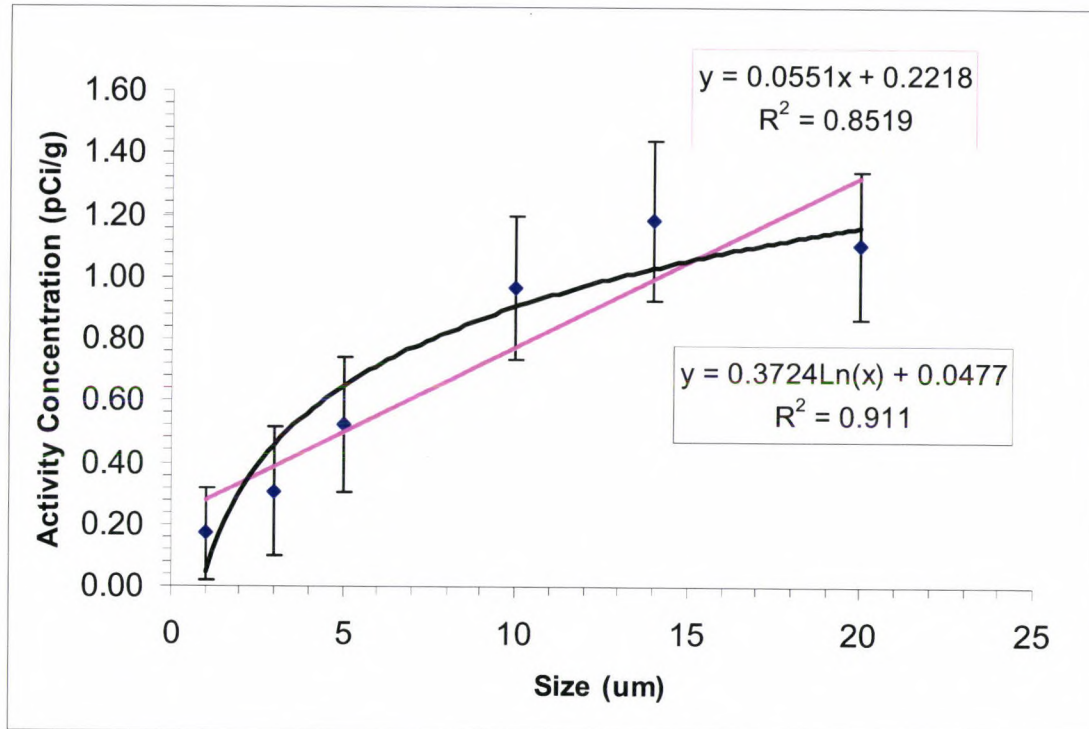


Fig. 3.8: Relationship between gross alpha activity concentration in fly ash (pCi g^{-1}) and particle aerodynamic diameter (μm) with error bars representing one standard deviation

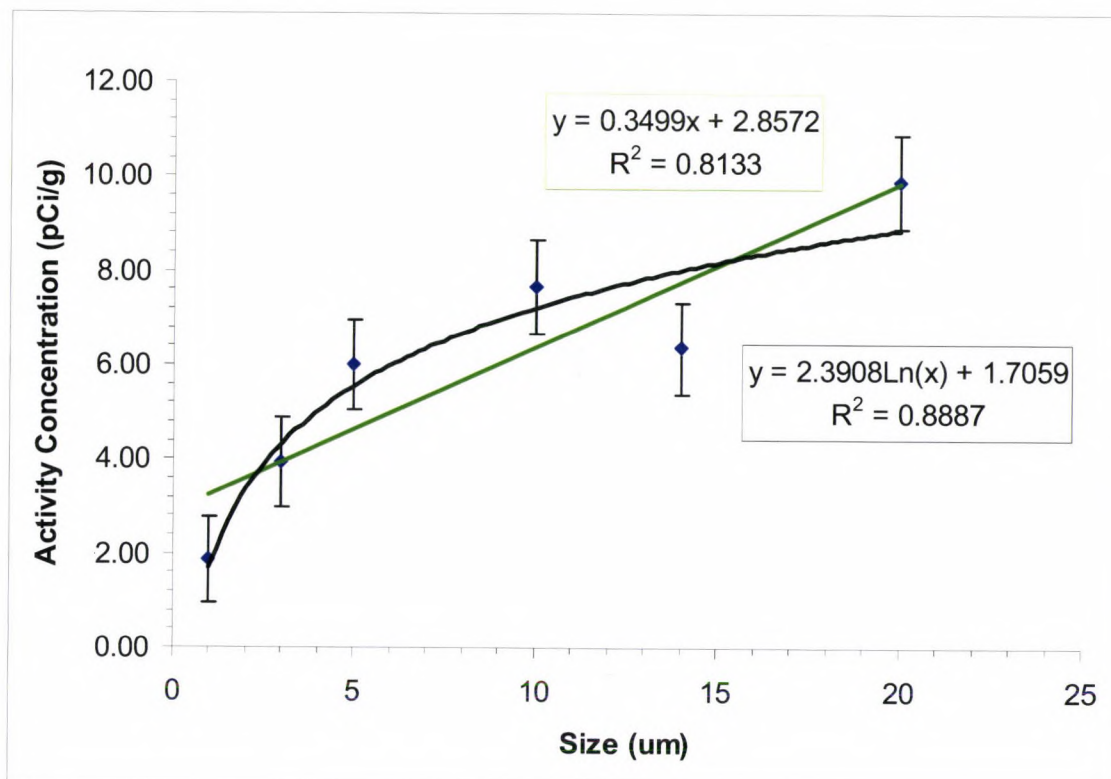


Fig. 3.9: Relationship between gross beta activity concentration in fly ash (pCi g^{-1}) and particle aerodynamic diameter (μm) with error bars representing one standard deviation

3.6 Radiochemical Analysis Data

3.6.1 Mass Spectroscopy Results

Prior to radiochemical analysis, raw (not size fractionated) fly ash was analyzed for elemental uranium and thorium (Table 3.4). This was accomplished using inductively coupled plasma mass spectroscopy (ICPMS).

Table 3.4: ICPMS results for elemental U and Th

Element	Concentration of Element in Fly Ash ($\mu\text{g/kg}$)
U	5100
Th	14000

The activity concentration of ^{238}U and ^{232}Th in the raw fly ash material were reported using ICPMS (Table 3.6).

Table 3.6: Activity concentration of ^{238}U and ^{232}Th in raw fly ash

Element	Activity Concentration of isotope in Fly Ash (pCi/g)
^{238}U	1.7
^{232}Th	1.5

3.6.2 Alpha Spectroscopy Results

The size fractionated fly ash aliquots were acid digested as described in section 2.2.3 and analyzed for isotopic uranium and thorium. Analytical losses in the 1 μm size fraction aliquot resulted in an insufficient amount of sample mass to meet the minimum detectable concentration (MDC) levels for both isotopic uranium and thorium. Therefore, the 1 μm aliquot was analyzed for isotopic uranium only.

The activity concentrations (Bq g^{-1}) of each sample and associated two standard deviations were recorded. The MDCs of ^{238}U and ^{232}Th for each size fraction were also recorded. All values were background corrected, the errors were propagated, and activity per unit mass calculated (Bq g^{-1} and pCi g^{-1}) (Tables 3.7 and 3.8). The concentration of ^{232}Th present in the 1 μm size fraction was determined by finding the ratio of ^{238}U to ^{232}Th for the other size fractions (range 1.16 to 1.75), averaging these values and finding the standard deviation, 2σ (1.44 and 0.48, respectively), and then estimating the concentration. The error was propagated for each step and calculated standard deviations are listed in Table 3.8.

Table 3.7: Activity concentration in each size fraction for ²³⁸U

Size (µm)	BACKGROUND CORRECTED SAMPLE			BACKGROUND CORRECTED SAMPLE		
	Activity Conc. (Bq g ⁻¹)	2σ (Bq g ⁻¹)	MDAC (Bq g ⁻¹)	Activity Conc. (pCi g ⁻¹)	2σ (pCi g ⁻¹)	MDAC (pCi g ⁻¹)
1	0.0176	0.0034	0.0006	0.4757	0.0924	0.0162
3	0.0382	0.0069	0.0007	1.0325	0.1867	0.0189
5	0.0492	0.0083	0.0005	1.3299	0.2245	0.0135
10	0.0640	0.0110	0.0010	1.7299	0.2975	0.0270
14	0.0670	0.0110	0.0010	1.8110	0.2975	0.0270
20	0.0690	0.0110	0.0010	1.8651	0.2975	0.0270

Table 3.8: Activity concentration in each size fraction for ²³²Th

Size (µm)	BACKGROUND CORRECTED SAMPLE			BACKGROUND CORRECTED SAMPLE		
	Activity Conc. (Bq g ⁻¹)	2σ prop. (Bq g ⁻¹)	MDAC (Bq g ⁻¹)	Activity Conc. (pCi g ⁻¹)	2σ (pCi g ⁻¹)	MDAC (pCi g ⁻¹)
1	0.012	0.073	n/a	0.329	1.962	n/a
3	0.024	0.025	0.002	0.647	0.059	0.059
5	0.028	0.029	0.002	0.761	0.062	0.062
10	0.044	0.044	0.001	1.180	0.038	0.038
14	0.053	0.054	0.001	1.445	0.027	0.027
20	0.059	0.060	0.001	1.607	0.027	0.027

3.7 ²³⁸U and ²³²Th Activity Concentration vs. Particle Size

The radiochemical analysis data were plotted as activity concentration (pCi g⁻¹) vs. size (µm). Activity concentration increases with increasing particle size for both nuclides. Both linear and non linear regressions were examined to ascertain the best fit to the data. As seen in Figures 3.8-3.9, these data follow a non-linear trend.

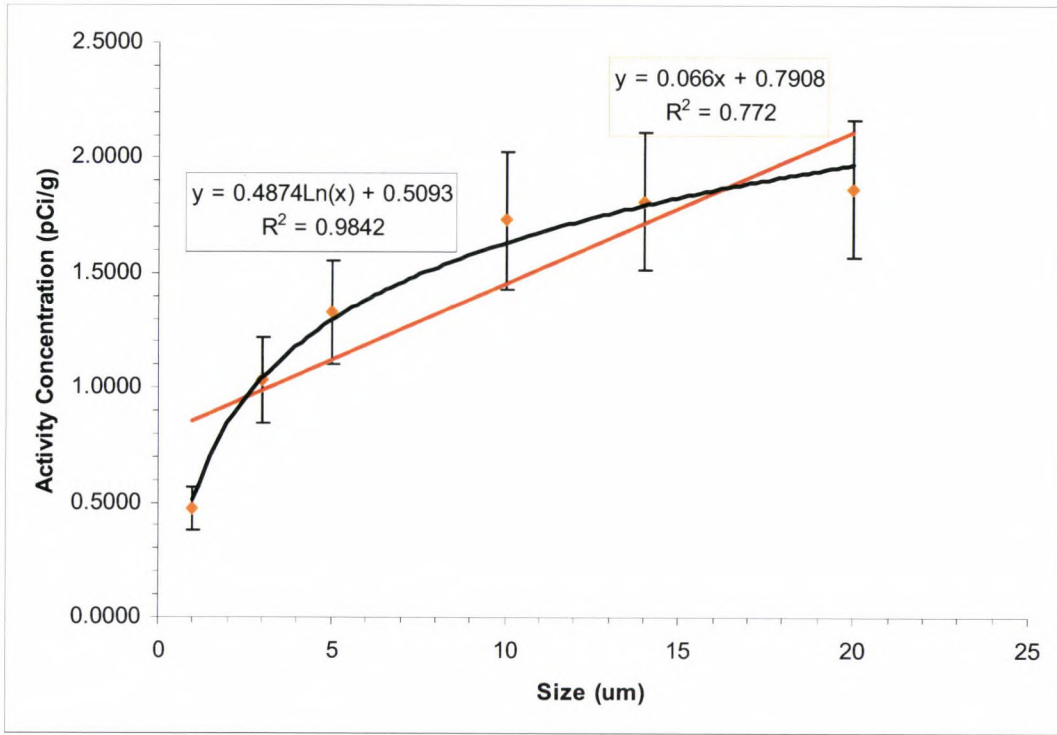


Figure 3.10: ^{238}U activity concentration vs. aerodynamic diameter for alpha spectroscopy data with error bars representing two standard deviations

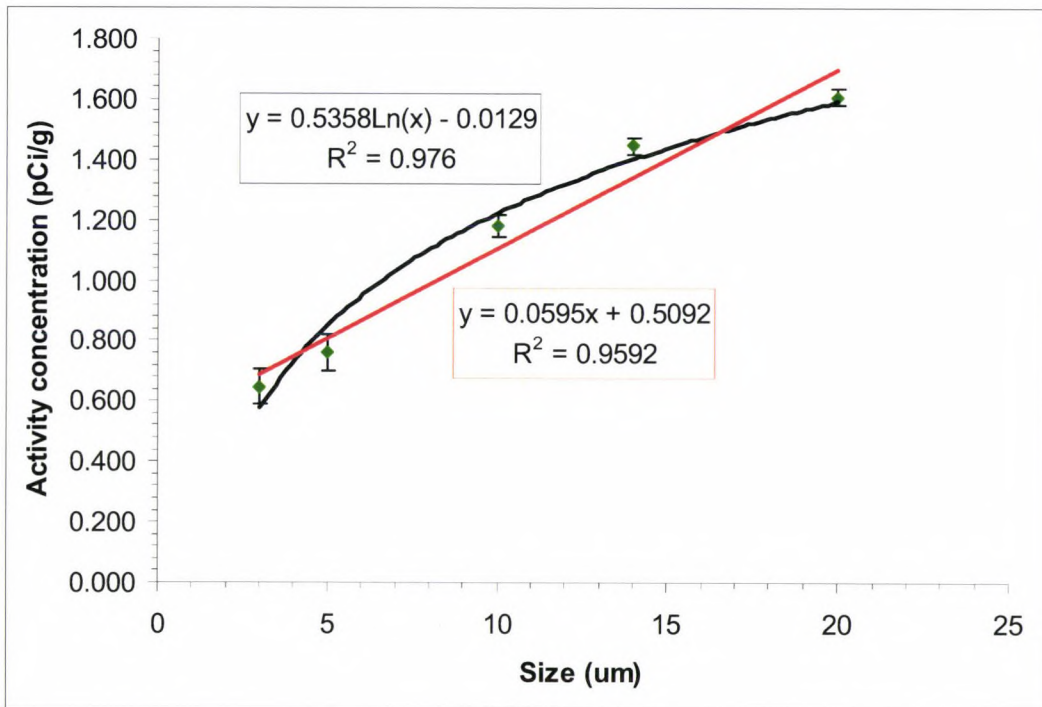


Figure 3.11: ^{232}Th activity concentration vs. aerodynamic diameter for alpha spectroscopy data with error bars representing two standard deviations

3.8 Activity Median Aerodynamic Diameter

The AMADs for both ^{238}U and ^{232}Th were calculated using the methodology described in section 2.2.4. The AMAD associated with ^{238}U and ^{232}Th are 7.8 μm with a geometric standard deviation (GSD) of 2.9 and 10.5 with a GSD of 3.5, respectively. These values and the corresponding ALIs from 10 CFR 20 were used to determine the inhalation committed effective dose equivalents (CEDE).

3.9 Dose Based on Inhaled Fly Ash Particulate Matter

3.9.1 Calculating Committed Effective Dose Equivalent

DFINT ©1992 (ver 4.1, Oak Ridge, TN) “A Code to Preview the Dosimetric Data of ICRP Publication 30, parts 1-4” written by Keith Eckerman was used to determine the CEDE (ICRP 30 and 60) for intakes of ^{238}U and ^{232}Th . Particle deposition fractions within the lung change according to the AMAD, and the CEDE is adjusted accordingly. The changes in deposition fraction are listed in Table 3.9. DFINT requires particle size input to recalculate the CEDE.

Table 3.9: Changes in deposition fraction with varying AMAD

AMAD (μm)	Region of Deposition	Deposition Fraction (%)
1	nasopharyngeal	30.0
	tracheobronchial	8.0
	pulmonary	25.0
7.8	nasopharyngeal	83.4
	tracheobronchial	8.0
	pulmonary	6.2
10.5	nasopharyngeal	88.2
	tracheobronchial	7.5
	pulmonary	4.7

Dose was calculated and reported for the three different solubility classes since the solubility was unknown: D, W, and Y (F, M, and S for ICRP 60). The CEDE was calculated by summing the product of tissue weighting factors and the committed dose equivalent (CDE) for various tissues and organs. The CDE for each organ changes with solubility class. Remainder organ dose also changes with solubility class. The listed organs and tissue weighting factors for ICRP 30 are slightly different than for ICRP 60, so each is listed and calculated separately.^{60,61} The CDE per inhaled μCi of activity for each listed organ was recorded and listed in Tables 3.10-3.13. The CEDEs for ICRP 30⁶⁰ and 60⁶¹ models are compiled in Table 3.14.

Table 3.10: ICRP 30 CDEs for ^{238}U , class D, W, Y

CLASS D			
Organ	CDE (rem μCi^{-1})	Organ	CDE (rem μCi^{-1})
Adrenals	9.97E-02	Lungs	3.49E-01
Bladder Wall	9.88E-02	Ovaries	9.93E-02
Bone Surface	4.35E+01	Pancreas	9.93E-02
Breast	9.93E-02	R Marrow	2.92E+00
ST wall	9.97E-02	Skin	9.93E-02
SI wall	1.02E-01	Spleen	9.93E-02
ULI wall	1.19E-01	Testes	9.88E-02
LLI wall	1.64E-01	Thymus	9.88E-02
Kidneys	1.78E+01	Thyroid	9.88E-02
Liver	9.88E-02	Uterus	9.88E-02
Remainder	3.67E+00		

CLASS W			
Organ	CDE (rem μCi^{-1})	Organ	CDE (rem μCi^{-1})
Adrenals	3.06E-02	Lungs	1.29E+01
Bladder Wall	3.03E-02	Ovaries	3.04E-02
Bone Surface	1.33E+01	Pancreas	3.05E-02
Breast	3.05E-02	R Marrow	8.97E-01
ST wall	3.33E-02	Skin	3.04E-02
SI wall	3.80E-02	Spleen	3.05E-02
ULI wall	7.46E-02	Testes	3.03E-02
LLI wall	1.68E-01	Thymus	3.06E-02
Kidneys	5.48E+00	Thyroid	3.04E-02
Liver	3.05E-02	Uterus	3.03E-02
Remainder	1.16E+00		

CLASS Y			
Organ	CDE (rem μCi^{-1})	Organ	CDE (rem μCi^{-1})
Adrenals	4.53E-03	Lungs	2.42E+02
Bladder Wall	3.86E-03	Ovaries	3.93E-03
Bone Surface	1.64E+00	Pancreas	4.47E-03
Breast	4.50E-03	R Marrow	1.11E-01
ST wall	7.93E-03	Skin	3.94E-03
SI wall	1.30E-02	Spleen	4.39E-03
ULI wall	5.78E-02	Testes	3.84E-03
LLI wall	1.71E-01	Thymus	4.96E-03
Kidneys	6.93E-01	Thyroid	4.17E-03
Liver	4.00E-03	Uterus	3.89E-03
Remainder	1.89E-01		

Table 3.11: ICRP 60 CDEs ^{238}U , class F(D), M(W), S(Y)

CLASS D			
Organ	CDE (rem μCi^{-1})	Organ	CDE (rem μCi^{-1})
Adrenals	9.97E-02	Lungs	3.49E-01
Bladder Wall	9.88E-02	Ovaries	9.93E-02
Bone Surface	4.35E+01	Pancreas	9.93E-02
Breast	9.93E-02	R Marrow	2.92E+00
ST wall	9.97E-02	Skin	9.93E-02
SI wall	1.02E-01	Spleen	9.93E-02
ULI wall	1.19E-01	Testes	9.88E-02
LLI wall	1.64E-01	Thymus	9.88E-02
Kidneys	1.78E+01	Thyroid	9.88E-02
Liver	9.88E-02	Uterus	9.88E-02
Remainder	2.86E-01		

CLASS W			
Organ	CDE (rem μCi^{-1})	Organ	CDE (rem μCi^{-1})
Adrenals	3.06E-02	Lungs	1.29E+01
Bladder Wall	3.03E-02	Ovaries	3.04E-02
Bone Surface	1.33E+01	Pancreas	3.05E-02
Breast	3.05E-02	R Marrow	8.97E-01
ST wall	3.33E-02	Skin	3.04E-02
SI wall	3.80E-02	Spleen	3.05E-02
ULI wall	7.46E-02	Testes	3.03E-02
LLI wall	1.68E-01	Thymus	3.06E-02
Kidneys	5.48E+00	Thyroid	3.04E-02
Liver	3.05E-02	Uterus	3.03E-02
Remainder	8.83E-02		

CLASS Y			
Organ	CDE (rem μCi^{-1})	Organ	CDE (rem μCi^{-1})
Adrenals	4.53E-03	Lungs	2.42E+02
Bladder Wall	3.86E-03	Ovaries	3.93E-03
Bone Surface	1.64E+00	Pancreas	4.47E-03
Breast	4.50E-03	R Marrow	1.11E-01
ST wall	7.93E-03	Skin	3.94E-03
SI wall	1.30E-02	Spleen	4.39E-03
ULI wall	5.78E-02	Testes	3.84E-03
LLI wall	1.71E-01	Thymus	4.96E-03
Kidneys	6.93E-01	Thyroid	4.17E-03
Liver	4.00E-03	Uterus	3.89E-03
Remainder	1.22E-02		

Table 3.12: ICRP 30 CDEs ^{232}Th , class W, Y

CLASS W			
Organ	CDE (rem μCi^{-1})	Organ	CDE (rem μCi^{-1})
Adrenals	3.33E+00	Lungs	1.22E+01
Bladder Wall	3.07E+00	Ovaries	3.16E+00
Bone Surface	4.61E+04	Pancreas	3.18E+00
Breast	3.20E+00	R Marrow	3.71E+03
ST wall	3.07E+00	Skin	3.14E+00
SI wall	3.13E+00	Spleen	3.12E+00
ULI wall	3.12E+00	Testes	3.13E+00
LLI wall	3.24E+00	Thymus	3.12E+00
Kidneys	3.18E+00	Thyroid	3.09E+00
Liver	2.58E+01	Uterus	3.10E+00
Remainder	7.77E+00		

CLASS Y			
Organ	CDE (rem μCi^{-1})	Organ	CDE (rem μCi^{-1})
Adrenals	6.51E-01	Lungs	6.52E+02
Bladder Wall	6.03E-01	Ovaries	6.14E-01
Bone Surface	6.78E+03	Pancreas	6.37E-01
Breast	6.30E-01	R Marrow	5.45E+02
ST wall	6.22E-01	Skin	6.17E-01
SI wall	6.14E-01	Spleen	6.28E-01
ULI wall	6.82E-01	Testes	6.10E-01
LLI wall	7.71E-01	Thymus	6.46E-01
Kidneys	6.23E-01	Thyroid	6.15E-01
Liver	5.17E+00	Uterus	6.08E-01
Remainder	1.59E+00		

Table 3.13: ICRP 60 CDEs ²³²Th, class M(W), S(Y)

CLASS W			
Organ	CDE (rem μCi^{-1})	Organ	CDE (rem μCi^{-1})
Adrenals	3.33E+00	Lungs	1.22E+01
Bladder Wall	3.07E+00	Ovaries	3.16E+00
Bsurface	4.61E+04	Pancreas	3.18E+00
Breast	3.20E+00	R Marrow	3.71E+03
ST wall	3.07E+00	Skin	3.14E+00
SI wall	3.13E+00	Spleen	3.12E+00
ULI wall	3.12E+00	Testes	3.13E+00
LLI wall	3.24E+00	Thymus	3.12E+00
Kidneys	3.18E+00	Thyroid	3.09E+00
Liver	2.58E+01	Uterus	3.10E+00
Remainder	3.21E+00		

CLASS Y			
Organ	CDE (rem μCi^{-1})	Organ	CDE (rem μCi^{-1})
Adrenals	6.51E-01	Lungs	6.52E+02
Bladder Wall	6.03E-01	Ovaries	6.14E-01
Bsurface	6.78E+03	Pancreas	6.37E-01
Breast	6.30E-01	R Marrow	5.45E+02
ST wall	6.22E-01	Skin	6.17E-01
SI wall	6.14E-01	Spleen	6.28E-01
ULI wall	6.82E-01	Testes	6.10E-01
LLI wall	7.71E-01	Thymus	6.46E-01
Kidneys	6.23E-01	Thyroid	6.15E-01
Liver	5.17E+00	Uterus	6.08E-01
Remainder	6.30E-01		

Table 3.14: CEDE by radionuclide, model, and class

Radionuclide	Model	Class	CEDE (rem μCi^{-1})
²³⁸ U	ICRP 30	D	2.84
		W	2.42
		Y	29.2
	ICRP 60	F	0.921
		M	1.84
		S	29.1
²³² Th	ICRP 30	W	1830
		Y	348
	ICRP 60	M	912
		S	212

3.9.2 Dose Received by Inhaled Mass

The mass of fly ash PM necessary to deliver the occupational limit of 5 rem per year was determined using the average activity concentration of ^{238}U and ^{232}Th for all size fractions. The CEDE associated with ^{238}U and ^{232}Th was then used to calculate dose per unit mass (Table 3.15).

Table 3.15: Average concentrations of ^{238}U and ^{232}Th

Radionuclide	Average Concentration (Bq g ⁻¹)	Average Concentration (pCi g ⁻¹)
^{238}U	0.05	1.37
^{232}Th	0.04	0.99

Dose (rem) per unit mass (g) calculation for ^{238}U using ICRP 30

Class D

$$\left(\frac{1.37 \text{ pCi}}{\text{g}}\right) \left(\frac{1 \mu\text{Ci}}{10^6 \text{ pCi}}\right) \left(\frac{2.84 \text{ rem}}{\mu\text{Ci}}\right) = \frac{3.89 \times 10^{-6} \text{ rem}}{\text{g}} \quad \text{Eqn 3.1}$$

Class W

$$\left(\frac{1.37 \text{ pCi}}{\text{g}}\right) \left(\frac{1 \mu\text{Ci}}{10^6 \text{ pCi}}\right) \left(\frac{2.42 \text{ rem}}{\mu\text{Ci}}\right) = \frac{3.32 \times 10^{-6} \text{ rem}}{\text{g}} \quad \text{Eqn 3.2}$$

Class Y

$$\left(\frac{1.37 \text{ pCi}}{\text{g}}\right) \left(\frac{1 \mu\text{Ci}}{10^6 \text{ pCi}}\right) \left(\frac{29.2 \text{ rem}}{\mu\text{Ci}}\right) = \frac{4.00 \times 10^{-5} \text{ rem}}{\text{g}} \quad \text{Eqn 3.3}$$

Dose (rem) per unit mass (g) calculation for ^{232}Th using ICRP 30

Class W

$$\left(\frac{0.99 \text{ pCi}}{\text{g}}\right) \left(\frac{1 \mu\text{Ci}}{10^6 \text{ pCi}}\right) \left(\frac{1830 \text{ rem}}{\mu\text{Ci}}\right) = \frac{1.81 \times 10^{-3} \text{ rem}}{\text{g}} \quad \text{Eqn 3.4}$$

Class Y

$$\left(\frac{0.99 \text{ pCi}}{\text{g}}\right)\left(\frac{1 \mu\text{Ci}}{10^6 \text{ pCi}}\right)\left(\frac{348 \text{ rem}}{\mu\text{Ci}}\right) = \frac{3.44 \times 10^{-4} \text{ rem}}{\text{g}} \quad \text{Eqn 3.5}$$

Dose (rem) per unit mass (g) calculation for ^{238}U using ICRP 60

Class F

$$\left(\frac{1.37 \text{ pCi}}{\text{g}}\right)\left(\frac{1 \mu\text{Ci}}{10^6 \text{ pCi}}\right)\left(\frac{0.92 \text{ rem}}{\mu\text{Ci}}\right) = \frac{1.26 \times 10^{-6} \text{ rem}}{\text{g}} \quad \text{Eqn 3.6}$$

Class M

$$\left(\frac{1.37 \text{ pCi}}{\text{g}}\right)\left(\frac{1 \mu\text{Ci}}{10^6 \text{ pCi}}\right)\left(\frac{1.84 \text{ rem}}{\mu\text{Ci}}\right) = \frac{2.52 \times 10^{-6} \text{ rem}}{\text{g}} \quad \text{Eqn 3.7}$$

Class S

$$\left(\frac{1.37 \text{ pCi}}{\text{g}}\right)\left(\frac{1 \mu\text{Ci}}{10^6 \text{ pCi}}\right)\left(\frac{29.1 \text{ rem}}{\mu\text{Ci}}\right) = \frac{3.99 \times 10^{-5} \text{ rem}}{\text{g}} \quad \text{Eqn 3.8}$$

Dose (rem) per unit mass (g) calculation for ^{232}Th using ICRP 60

Class M

$$\left(\frac{0.99 \text{ pCi}}{\text{g}}\right)\left(\frac{1 \mu\text{Ci}}{10^6 \text{ pCi}}\right)\left(\frac{912 \text{ rem}}{\mu\text{Ci}}\right) = \frac{9.03 \times 10^{-4} \text{ rem}}{\text{g}} \quad \text{Eqn 3.9}$$

Class S

$$\left(\frac{0.99 \text{ pCi}}{\text{g}}\right)\left(\frac{1 \mu\text{Ci}}{10^6 \text{ pCi}}\right)\left(\frac{212 \text{ rem}}{\mu\text{Ci}}\right) = \frac{2.10 \times 10^{-4} \text{ rem}}{\text{g}} \quad \text{Eqn 3.10}$$

According to the literature, radioactive equilibrium does not exist between ^{238}U and ^{226}Ra in fly ash.^{33, 62} Dose per unit mass can not be calculated for other radionuclides in the decay chains as the data is lacking in this study. A Table is provided of these doses per unit mass for simplicity, Table 3.15.

Table 3.16: Dose per unit mass by nuclide, model, and class

Radionuclide	Model	Class	Dose per unit mass (rem g ⁻¹)
²³⁸ U	ICRP 30	D	3.89E-06
		W	3.32E-06
		Y	4.00E-05
	ICRP 60	F	1.26E-06
		M	2.52E-06
		S	3.99E-05
²³² Th	ICRP 30	W	1.81E-03
		Y	3.44E-04
	ICRP 60	M	9.03E-04
		S	2.10E-04

Chapter 4: Discussion

4.1 Discussion of Fly Ash Particle Size Distribution

Typical median diameters of stack fly ash particulate are listed in Table 4.1. After truncation, the MMAD calculated for the fly ash from this study sample was 7.4 μm with a GSD of 2.5 (section 3.4). These results were compared with results from studies where stack fly ash were sized (Table 4.1). The MMAD found in this study was found within the range listed in Table 4.1.

Table 4.1: Mass median diameters found in the literature for stack fly ash

Mass Median Diameter (μm)	Reference
2.4, 3.7, 6.0, 18.5	Coles et. al. ³³

The study in Table 4.1 utilized a cyclone for particle sizing. Small particles do not have enough inertia to impact on the cyclone wall; therefore a cyclone is not as efficient at differentiating small particle sizes. This is a limitation of the device and the Coles study. The aforementioned comparison is a possible limitation of the study described in this document.

4.2 Discussion of Radiochemical Analysis

The concentration of elemental thorium is 2.75 times greater than the concentration of elemental uranium in fly ash used in this study. This compares well with the range of ratios of elemental thorium to elemental

uranium found in literature (Table 4.2). These ratios were calculated using the data found in Table 1.5.

Table 4.2: Ratios of Th:U in fly ash from the literature

Elemental Ratio	Ratio	Reference
Th:U	2.68	Coles et. al.
	2.00	Coles et. al.
	3.33	Affolter et. al.
	2.97	Affolter et. al.
	3.06	Affolter et. al.
	3.11	Affolter et. al.

The activity concentration of ^{238}U and ^{232}Th in Table 3.6 compared to those in Table 1.8 suggest that the average concentration of ^{238}U and ^{232}Th found in the literature are 3.7 and 5 times greater than the respective activity concentrations of ^{238}U and ^{232}Th in this study.

4.3 Uncertainties in the Dose Calculation

Activity concentration of ^{238}U in fly ash increases with decreasing particle size according to the literature.^{12, 33, 62} While data in the literature are lacking for ^{232}Th , Weng and Chu also report that activity concentration increases with decreasing particle size for ^{228}Th (a daughter product of ^{232}Th).¹² These aforementioned relationships do not reflect the results in section 3.4 and 3.6. The AMAD was recalculated and CEDE for this study was adjusted based on the particle size reported by Weng and Chu. A size correction was applied using the percent increase found between activity concentrations in the size fractions from this study and the Weng and Chu study (Appendix G, Tables G.1 and G.2). The recalculated AMAD for ^{238}U

was 3.4 μm with a GSD of 3.52 and ^{232}Th was calculated to be 3.6 μm with a GSD of 4.4. The revised deposition fractions are listed in Table 4.3, based on ICRP 30. The CEDE for ^{238}U and ^{232}Th are listed in Table 4.4.

Table 4.3: Changes in deposition fraction using re-calculated AMAD

Size (um)	Region of Deposition	Deposition Fraction (%)
3.4	nasopharyngeal	64.8
	tracheobronchial	8.0
	pulmonary	11.7
3.6	nasopharyngeal	66.3
	tracheobronchial	8.0
	pulmonary	11.2

Table 4.4: CEDE by radionuclide, model, and class

Radionuclide	Model	Class	CEDE (rem μCi^{-1})
^{238}U	ICRP 30	D	2.65
		W	3.75
		Y	55.4
	ICRP 60	F	0.876
		M	3.21
		S	55.3
^{232}Th	ICRP 30	W	1750
		Y	603
	ICRP 60	M	871
		S	394

The dose per unit mass for ^{238}U and ^{232}Th was calculated using the literature based AMAD corrected CEDEs per section 3.8.2 and the data from Table 3.15. The revised doses per unit mass inhaled are reported in Table 4.5.

Table 4.5: Dose per unit mass by nuclide, model, and class

Radionuclide	Model	Class	Dose per unit mass (rem g ⁻¹)
²³⁸ U	ICRP 30	D	3.63E-06
		W	5.14E-06
		Y	8.00E-05
	ICRP 60	F	1.20E-06
		M	4.40E-06
		S	8.00E-05
²³² Th	ICRP 30	W	1.73E-03
		Y	6.00E-04
	ICRP 60	M	8.60E-04
		S	3.90E-04

4.4 Explanation for the Trends in the Gross Alpha and Beta Count Rate vs. Mass Data

4.4.1 Explanation for the Trends in the Gross Alpha Count Rate vs. Mass

The most likely explanation for the trend described in section 3.3.1a is that alpha particles are being absorbed in the fly ash material (with absorption increasing as a function of mass) and are unable to penetrate to the detector. As fly ash mass increases in the planchet, the depth of fly ash also increases beyond the range of the alpha particles emitted. This is a reasonable explanation for the asymptotic phenomenon seen in Figure 4.2. The range of the highest energy ²³⁸U alpha particle in fly ash is 23-24 μm. The ²³²Th alpha particle energies are all less than the ²³⁸U alpha emissions and were not considered.⁶⁴ Range calculations for ²³⁸U are provided below.

Range in air for a ^{238}U alpha particle for energies between 2-8 MeV⁵⁰

$$R_{\text{air}} (\text{cm}) = 0.322 [E (\text{MeV})]^{3/2} \quad (\text{Eqn 4.1})$$

Upper bound 79% yield: 4.197 MeV⁶⁴

$$R_{\text{air}} (\text{cm}) = 0.322 (4.197 \text{ MeV})^{3/2} = 2.76 \text{ cm}$$

Lower bound 0.078% yield: 4.038 MeV⁶⁴

$$R_{\text{air}} (\text{cm}) = 0.322 (4.038 \text{ MeV})^{3/2} = 2.61 \text{ cm}$$

The range in fly ash for a ^{238}U alpha particle assuming fly ash has a density of 2 g cm^{-3} and molecular weight that of SiO_2

$$R_{\text{flyash}} = \frac{R_{\text{air}} \times \rho_{\text{air}} \times (A_{\text{flyash}})^{1/2}}{\rho_{\text{flyash}} \times (A_{\text{air}})^{1/2}} \quad (\text{Eqn 4.2})$$

Upper bound

$$R_{\text{flyash}} = \frac{(2.76 \text{ cm}) \times (1.21 \times 10^{-3} \text{ g/cm}^3) \times (60 \text{ g/mol})^{1/2}}{(2 \text{ g/cm}^3) \times (29 \text{ g/mol})^{1/2}} = 2.4 \times 10^{-3} \text{ cm or } 24 \text{ } \mu\text{m}$$

Lower bound

$$R_{\text{flyash}} = \frac{(2.61 \text{ cm}) \times (1.21 \times 10^{-3} \text{ g/cm}^3) \times (60 \text{ g/mol})^{1/2}}{(2 \text{ g/cm}^3) \times (29 \text{ g/mol})^{1/2}} = 2.3 \times 10^{-3} \text{ cm or } 23 \text{ } \mu\text{m}$$

4.4.2 Explanation for the Trends in the Gross Beta Count Rate vs. Mass

The trend in the gross beta count rate vs. mass data indicates an increasing relationship between count rate and mass with more variability in lower masses than higher masses. This can be also seen in the residual plot, Figure 3.7.

4.4.3 *Gross Alpha and Beta Counting for Dose Assessment*

Gross alpha and beta counting is not the ideal method for calculating activity concentrations of ^{238}U and ^{232}Th in fly ash. These counting techniques do not allow identification of nuclides, making it difficult to determine dose. It would be necessary to couple gross alpha and beta counting with techniques such as quantitative gamma spectroscopy to determine the isotopes present. Gross counting is suboptimal for identifying alpha and beta particles emanating from fly ash. Acid digestion of samples is required to minimize self absorption of alpha particles when measuring gross counts. Gross alpha counting is best used to determine whether fly ash is radioactive and what mass is required to statistically detect radioactivity.

4.5 Activity Concentration vs. Particle Size Relationship

A non-linear relationship between activity concentration and particle size can be seen in Figures 3.8-3.11 and it is unclear why this was the resulting trend. It is possible that smaller particles interacted with sodium hexametaphosphate during the sizing process, causing a change in the solubility of ^{238}U and ^{232}Th in the fly ash. All samples of fly ash were digested during radiochemical analysis or destroyed during a laboratory accident, so no follow up experiments to resolve this issue were possible. During particle sizing at the Soils Laboratory, all samples were blank corrected for the mass of the sodium hexametaphosphate. However, if the mass of the sodium hexametaphosphate is much greater than that of the particles, there is a

greater chance for mass contamination of sodium hexametaphosphate on the particles. This would attenuate the alpha particles and they would not be detected. The blank correction calculations could not to be obtained from the Soils Laboratory. Further investigation is a task for future studies.

4.6 Dose Assessment and Risk from Inhalation of Fly Ash Material

4.6.1 Dose Assessment and Risk using Data Provided by Radiochemical Analysis

Doses to workers and the public were calculated for inhaled masses ranging from 10^{-6} g – 10^1 g using data from Table 3.15. Doses were estimated using ICRP 30⁶⁰ and ICRP 60⁶¹ models (Appendix A, Table A.2). The ICRP detriment coefficients, defined as “a coefficient that represents the combination of the probability of occurrence of a harmful health effect and also a judgement of the severity of the effect per unit dose,⁶¹” were used to estimate the harmful effect produced by inhalation of 1 g of fly ash PM (Table 4.6).⁵⁰ Harmful effects are delineated by the ICRP as the following: dying from cancer, being diagnosed with non-fatal cancer, or manifesting severe hereditary effects. The increased risk (in percentage) of these aforementioned harmful effects is listed in Tables 4.7 and 4.8.

Table 4.6: Detriment coefficients for stochastic effects

Exposed Population	Detriment ($\times 10^{-4} \text{ rem}^{-1}$)		
	Fatal Cancer	Non-Fatal Cancer	Severe Hereditary Effects
Entire population	5	1	1.3

Table 4.7: ICRP 30 increased risk from inhalation of 1 g of fly ash

Radionuclide	Class	Increased risk from inhalation of 1 g of fly ash		
		Fatal CA (%)	Non-fatal CA (%)	Severe Hereditary Effects (%)
²³⁸ U	D	1.95E-07	3.89E-08	5.06E-08
	W	1.66E-07	3.32E-08	4.31E-08
	Y	2.00E-06	4.00E-07	5.20E-07
²³² Th	W	9.06E-05	1.81E-05	2.36E-05
	Y	1.72E-05	3.45E-06	4.48E-06

Table 4.8: ICRP 60 increased risk from inhalation of 1 g of fly ash

Radionuclide	Class	Increased Risk from inhalation of 1 g of fly ash		
		Fatal CA (%)	Non-fatal CA (%)	Severe Hereditary Effects (%)
²³⁸ U	F	6.31E-08	1.26E-08	1.64E-08
	M	1.26E-07	2.52E-08	3.28E-08
	S	1.99E-06	3.99E-07	5.18E-07
²³² Th	M	4.51E-05	9.03E-06	1.17E-05
	S	1.05E-05	2.10E-06	2.73E-06

The mass of fly ash necessary to reach the occupational limit of 5 rem per year and the public limit of 100 mrem per year⁵⁰ was calculated and results listed in Appendix A, Table A.1.

4.6.2 Dose Assessment and Risk using Data Provided by Radiochemical Analysis Accounting for Uncertainties

Dose and risk were assessed in a similar fashion as described in section 4.6.1, using the data in section 4.3. The increase in risk from inhalation of 1 gram of fly ash material is listed in Tables 4.9-4.10. The mass necessary to reach the occupational limit and public limit is listed in Appendix B, Table B.1.

Table 4.9: ICRP 30 increased risk of stochastic effect from inhalation of 1 g of fly ash accounting for size uncertainties

Radionuclide	Class	Increased risk from inhalation of 1 g of fly ash		
		Fatal CA (%)	Non-fatal CA (%)	Severe Hereditary Effects (%)
²³⁸ U	D	1.82E-07	3.63E-08	4.72E-08
	W	2.57E-07	5.14E-08	6.68E-08
	Y	4.00E-06	8.00E-07	1.04E-06
²³² Th	W	8.65E-05	1.73E-05	2.25E-05
	Y	3.00E-05	6.00E-06	7.80E-06

Table 4.10: ICRP 60 increased risk of stochastic effect from inhalation of 1 g of fly ash accounting for size uncertainties

Radionuclide	Class	Increased Risk from inhalation of 1 g of fly ash		
		Fatal CA (%)	Non-fatal CA (%)	Severe Hereditary Effects (%)
²³⁸ U	F	6.00E-08	1.20E-08	1.56E-08
	M	2.20E-07	4.40E-08	5.72E-08
	S	4.00E-06	8.00E-07	1.04E-06
²³² Th	M	4.30E-05	8.60E-06	1.12E-05
	S	1.95E-05	3.90E-06	5.07E-06

Application of a size correction factor during the calculation of AMAD as described in section 4.3 increases or decreases the risks associated with inhalation by approximately 10 percent in most cases. While the differences between the raw data in this study and the size adjusted data (based on the literature) are small, as previously mentioned, the actual dose contribution of ²³⁸U and ²³²Th to the overall CEDE and risk from fly ash inhalation is bound by the doses and risks calculated from these two data sets.

4.7 Further Research

Stack sampling within the Plant would provide a more representative size distribution of PM being dispersed into the atmosphere. A comparison of the results described in this report and stack sample results might be utilized

to make generalizations about stack effluent using samples from fabric filter or electrostatic precipitator fly ash. Bi-Gaussian plume modeling of the Plant effluent would provide insight on where the radionuclides may be inhaled or deposited downwind. Soil leaching and ground water studies of the area could provide information on the potential concentration and buildup of radioactivity from the fly ash and how radioactivity is transported within the ecosystem as well as ascertaining the risk to the environment.

Coal utilized by the Plant should be analyzed using the methodology in chapter 2 to ascertain if enrichment of the radionuclides of interest occurs during the coal combustion process. A determination could then be made as to whether coal fly ash should be classified as naturally occurring radioactive material (NORM) or technologically enhanced naturally occurring radioactive material (TENORM).

Simulated lung fluid should be used to help understand fly ash solubility and classification (D/F, W/M, Y/S) of the radionuclides present to aid in more accurate dose assessment. The potential environmental impact of fly ash storage could be determined by soil leaching studies and ground water studies. Colorado has a dry and windy climate so resuspension of fly ash material in these storage areas could pose a health risk to employees and the neighboring public. Accurate dose assessment requires understanding how fly ash is resuspended and transported. The various types of coal should be investigated to discover if radioactivity is related to other characteristics.

4.8 Conclusion

The results of this study indicate that fly ash is not a radioactive substance as defined by the IAEA safety standards and Title 49 Code of Federal Regulations.^{65, 66} Activity concentrations of ^{238}U and ^{232}Th that do not exceed the quantity 10 Bq g^{-1} (270.3 pCi g^{-1}) are considered exempt from radioactive material shipping requirements. Although the relative concentration of radionuclides in the fly ash of this study is quite low, it is still possible for individuals to receive a measurable dose.

Doses estimated using ICRP 30 are higher than those calculations utilizing ICRP 60 techniques due to the differences in tissue weighting factors. In order to exceed occupational and public dose limits, inhalation of approximately 1-1000 kg of fly ash for ^{238}U and approximately 50 g to 20 kg for ^{232}Th would be necessary (Appendix A, Tables A.2 and A.4). The highest CEDE (ICRP 30) per unit mass incurred by inhalation of fly ash was class W ^{232}Th (1.81 mrem g^{-1}), while class W ^{238}U has the lowest CEDE per unit mass ($3.32 \text{ } \mu\text{rem g}^{-1}$).

The general relationship between activity concentration of ^{238}U and ^{232}Th found using data from radiochemical analysis and particle size suggest that activity concentration increases with increasing particle size. However the relationship between activity concentration and particle size found in the literature suggests that activity concentration increases with decreasing particle size. The AMAD and CEDE were re-calculated using the assumption that activity concentration in ^{238}U and ^{232}Th increases with decreasing particle

size (section 4.3). The CEDE and risks described in section 4.3.1 do not increase or decrease significantly, although the deposition fraction and CDE for each organ changes. The dose contribution of ^{238}U and ^{232}Th to the overall CEDE from inhalation of fly ash is bound between the doses calculated using the raw data from this study and the size adjusted data from this study to reflect the literature.

The chance of dying from cancer or being diagnosed with non-fatal cancer or severe hereditary effects from an acute inhalation of 1 g of fly ash PM is very low (Tables 4.7-4.10). However, based on the linear, no-threshold model from BEIR VII there is still an increased risk of harmful effects by the inhalation of fly ash material.

References:

1. Aly, A.I.M., et al., *Radiation Doses Resulting from a Proposed Coal-Fired Power Plant in the Suez Canal Area*. Energy, 1994. **19**(1): p. 55-61.
2. Aycik, G.A. and A. Ercan, *Radioactivity Measurements of Coals and Ashes from Coal-Fired Power Plants in the Southwestern Part of Turkey*. Journal of Environmental Radioactivity, 1997. **35**(1): p. 23-35.
3. Beck, H.L., *Radiation Exposures Due to Fossil Fuel Combustion*. International Journal of Radiation Applications and Instrumentation. Part C. Radiation Physics and Chemistry, 1989. **34**(2): p. 285-293.
4. Chauhan, R.P., et al., *Measurement of Alpha Radioactive Air Pollutants in Fly Ash Brick Dwellings*. Radiation Measurements, 2003. **36**(1-6): p. 533-536.
5. Gabbard, A., *Coal Combustion: Nuclear Resource or Danger*, in ORNL Review. 1993.
6. Mishra, U.C., *Environmental Impact of Coal Industry and Thermal Power Plants in India*. Journal of Environmental Radioactivity, 2004. **72**(1-2): p. 35-40.
7. Pacyna, J.M., *Radionuclide Behavior in Coal-Fired Plants*. Ecotoxicology and Environmental Safety, 1980. **4**(3): p. 240-251.
8. Papastefanou, C., *Radiological Impact from Atmospheric Releases of Ra-226 from Coal-Fired Power Plants*. Journal of Environmental Radioactivity, 1996. **32**(1-2): p. 105-114.
9. Rausch, H., et al., *Distribution of Toxic and Radiation Components in Air Particulates*. The Science of the Total Environment, 1995. **173-174**: p. 283-291.
10. Tadmor, J., *Radioactivity From Coal-Fired Power Plants: A Review*. Journal of Environmental Radioactivity, 1986. **4**(3): p. 177-204.
11. Tracy, B.L. and F.A. Prantl, *Radiological Impact of Coal-Fired Power Generation*. Journal of Environmental Radioactivity, 1985. **2**(2): p. 145-160.
12. Weng, Y.-H. and T.-C. Chu, *Concentrations of Radionuclides of Size Fractionated Fly-Ash Emissions from a Thermal Power Plant Using Taiwan Coal*. Journal of Radiation Research, 1992. **33**(2): p. 141-150.
13. *State Energy Profiles: Colorado*. 2009 November 25 [cited 2009 November 30]; Available from: http://tonto.eia.doe.gov/state/state_energy_profiles.cfm?sid=CO.
14. *Title 10 - Energy, Code of Federal Regulations Part 20 - Standards for Protection Against Radiation, Appendix B*. 2009, Nuclear Regulatory Commission.
15. *How is Coal Formed?* 2006 [cited 2009 August 11]; Available from: <http://www.uky.edu/KGS/coal/coalform.htm>.
16. *Coal*. 2007 [cited 2009 August 6]; Available from: <http://www.epa.gov/RDEE/energy-and-you/affect/coal.html>.

17. *Classification and Rank of Coal*. 2006 [cited 2009 August 11]; Available from: <http://www.uky.edu/KGS/coal/coalkinds.htm>.
18. Thomas, L., *Coal Geology*. 2002: Wiley and Sons.
19. *Percent of Total U.S. Coal Production Mined from the Powder River Basin*. 2009 [cited 2009 October 26]; Available from: <http://www.blm.gov/pgdata/etc/medialib/blm/wy/programs/energy/coal/prb.Par.5321.Image.-1.-1.1.gif>
20. Bergemann, C. *PRB Coal Properties*. 2005 [cited 2009 October 26]; Available from: <http://www.cba-ssd.com/Applications/knowledgeBase/PRBcoal/PRBcoalProperty.htm>.
21. *Powder River Basin Coal Production*. 2009 [cited 2009 August 11]; Available from: http://www.blm.gov/wy/st/en/programs/energy/Coal_Resources/PRB_Coal/production.html.
22. Stricker, G.D. and M.S. Ellis, *Coal Quality and Geochemistry, Powder River Basin, Wyoming and Montana*. 1999, United States Geological Survey, Professional Paper 1625-A, Chapter PQ.
23. Affolter, R.H., M.E. Brownfield, and J.D. Cathcart. *Chemical Variation of Feed Coal and Coal Combustion Products from an Indiana Power Plant Utilizing Low Sulfur Powder River Basin Coal*. in *International Ash Utilization Symposium*. 1999. Center for Applied Energy Research, University of Kentucky.
24. *A Brief History of Coal Use*. 2008 [cited 2009 August 6]; Available from: http://fossil.energy.gov/education/energylessons/coal/coal_history.html
25. De Angelo, L. *London Smog Disaster, England*. 2008 [cited 2009 October 26]; Available from: http://www.eoearth.org/article/London_smog_disaster,_England.
26. *Electric Power Monthly, July 2009 Edition*. 2009 [cited 2009 August 7]; Available from: http://www.eia.doe.gov/cneaf/electricity/epm/epm_sum.html.
27. *Fact Sheet FS-163-97 - Radioactive Elements in Coal and Fly Ash: Abundance, Forms, and Environmental Significance*. 1997 [cited 2009 August 7]; Available from: <http://pubs.usgs.gov/fs/1997/fs169-97/FS-163-97.html>.
28. *Coal Mining and Transportation*. 2008 [cited 2009 August 6]; Available from: http://www.fe.doe.gov/education/energylessons/coal/coal_mining.html.
29. Employee, *Personal Communication: Facts about The Plant*. 2009.
30. Ragaini, R.C. and J.M. Ondov, *Trace-Element Emissions from Western U.S. Coal-Fired Power Plants*. *Journal of Radioanalytical Chemistry*, 1977. **37**(2): p. 679-691.
31. Orfanoudakis, N., A. Vakalis, and K. Krallis. *Emission Reduction Techniques and Economics in Coal-Fired Power Plants*. 2005 [cited 2010 January 21]; Available from: http://library.tee.gr/digital/m2069/m2069_orfanoudakis.pdf.

32. *Coal to Electricity: How it works*. Coal Utilization Research Council 2010 [cited 2010 February 22]; Available from: <http://www.coal.org/pdf/CoaltoElectricity.pdf>.
33. Coles, D.G., R.C. Ragaini, and J.M. Ondov, *Behavior of Natural Radionuclides in Western Coal-Fired Power Plants*. Environmental Science and Technology, 1978. **12**(4): p. 442-446.
34. McBride, J.P., et al., *Radiological Impact of Airborne Effluents of Coal-Fired and Nuclear Power Plants - ORNL-5315*, in Oak Ridge National Laboratory Chemical Technology Division. 1977: Oak Ridge, TN.
35. *Fact Sheet FS-038-02 - Characterization and Modes of Occurrence of Elements in Feed Coal and Fly Ash - An Integrated Approach*. 2002, United States Geological Survey.
36. UNSCEAR, *Sources, Effects, and Risks of Ionizing Radiation*. 1993, New York: United Nations Scientific Committee on the Effects of Atomic Radiation.
37. Corbett, J.O., *The Radiation dose from Coal Burning: A Review of Pathways and Data*. Radiation Protection Dosimetry, 1983. **4**(1): p. 5-19.
38. NCRP, *Report No 95 - Radiation Exposure of the U.S. Population from Consumer Products and Miscellaneous Sources*. 1987, Bethesda, MD: National Council on Radiation Protection.
39. Prybutok, V.R. and L.M. Gold, *Sensitivity Analysis for Power Industry Radionuclide Air Stack Emissions Leukemia Incidence Risk Comparison Models*. Journal of Hazardous Materials, 1991. **26**: p. 319-331.
40. *BEIR Report 6 - Health Effects of Exposure to Radon*. 1999, Washington, D.C.: National Academies Press.
41. *BEIR Report 7 - Health Risks from Exposure to Low Levels of Ionizing Radiation*. 2005, Washington, D.C.: National Academies Press.
42. NCRP, *Report No. 125 - Deposition, Retention and Dosimetry of Inhaled Radioactive Substances*. 1997, Bethesda, MD: National Council on Radiation Protection and Measurements.
43. Hinds, W.C., *Aerosol Technology: Properties, Behavior, and Measurement of Airborne Particles*. 2nd ed. 1999, New York: John Wiley and Sons.
44. ICRP, *Annals of the ICRP, Publication 66 - Human Respiratory Tract Model for Radiological Protection*. 1994, Tarrytown, NY: International Commission on Radiological Protection, Elsevier Science, Inc.
45. *Power Company Press Release*. 2004 [cited 2009 August 7].
46. *The Plant Fact Sheet*. 2009 [cited 2009 August 7].
47. *USGS Thorium and Uranium Decay Chains*. 2009 [cited 2010 March 22]; Available from: http://gulfsci.usgs.gov/tampabay/data/2_biogeochemical_cycles/images/decaychain.gif.
48. Tennelec, *Tennelec LB5100 Operation Manual*. 1982, Oak Ridge, TN: Tennelec.

49. ISO, *Determination of the Lower Limits of Detection and Decision for Ionizing Radiation Measurements - Part 1: Fundamentals and Applications to Counting Measurements, Without the Influence of Sample Treatment*. 2000: International Standards Organization, ISO 11020-1:2000.
50. Cember, H. and T. Johnson, *Introduction to Health Physics*. 4th ed. 2009, New York: McGraw-Hill.
51. *Methods of Soil Analysis - Part 1: Physical and Mineralogical Properties, Including Statistics of Measurement and Sampling*. Agronomy, ed. C.A. Black. Vol. 9. 1965, Madison, WI: American Society of Agronomy, Inc.
52. *The Occupational Environment: Its Evaluation, Control, and Management*. 2nd ed, ed. S.R. DiNardi. 2003, Fairfax, VA: American Industrial Hygiene Association (AIHA) Press.
53. *Standard Operating Procedure 773: Total Dissolution of Solids for the Radiochemical Determination of Actinides and Other Non-Volatile Radionuclides*. 2007, The Laboratory.
54. *Standard Operating Procedure 778: Actinides - Uranium, Plutonium, and Americium/Curium (Partial) Sequential Separation by Ion Exchange*. 2009, The Laboratory.
55. Knoll, G., *Radiation Detection Measurement*. 3rd ed. 2000, New York: John Wiley and Sons.
56. *Standard Operating Procedure 714: Analysis of Alpha Emitting Radionuclides by Alpha Spectrometry*. 2007, The Laboratory.
57. *Title 10 - Energy, Code of Federal Regulations Part 20.1301 - Standards for Protection Against Radiation*. 2009, Nuclear Regulatory Commission
58. Kahane, L., *Regression Basics*. 2001, Thousand Oaks, CA: Sage Publications, Inc.
59. Yi, H., et al., *Fine Particle and Trace Element Emissions from an Anthracite Coal-Fired Power Plant Equipped with a Bag-house in China*. *Fuel*, 2008. **87**: p. 2050-2057.
60. ICRP, *Annals of the ICRP, Publication 30 - Limits for Intakes of Radionuclides by Workers*. 1982, Oxford: International Commission on Radiological Protection, Pergamon Press.
61. ICRP, *Annals of the ICRP, Publication 60 - Recommendations of the International Commission on Radiological Protection*. 1991, Oxford: International Commission on Radiological Protection, Pergamon Press.
62. Papastefanou, C., *Escaping Radioactivity from Coal-Fired Power Plants (CPPs) Due to Coal Burning and the Associated Hazards: A Review*. *Journal of Environmental Radioactivity*, 2009. **In Press**.
63. Campbell, J.A., Laul, J.C., Nielson, K.K., and Smith, R.D., *Separation and Chemical Characterization of Finely-Sized Fly-Ash Particles*. *Analytical Chemistry*, 1978. **50**(8): p. 1032-1040.

64. ICRP, *Annals of the ICRP, Publication 38 - Radionuclide Transformations: Energy and Intensity of Emissions*. 1983, Oxford: International Commission on Radiological Protection, Pergamon Press.
65. *Title 49 - Transportation, Code of Federal Regulations Part 173.436 - General Requirements for Shipments and Packagings: Exempt material activity concentrations and exempt consignment activity limits for radionuclides*. 2010, Department of Transportation.
66. IAEA, *Regulations for the Safe Transport of Radioactive Material - No. ST-1*. 1996, Vienna: International Atomic Energy Agency.

Appendix A: ICRP 30 and 60 Dose Calculations

Table A.1: Mass inhaled to reach public and occupational limits, ICRP 30

ICRP 30			MASS INHALED TO REACH PUBLIC AND OCCPUATIONAL LIMITS	
Radionuclide	Class	Dose per unit mass (rem g ⁻¹)	Inhaled mass to receive 5 rem (g)	Inhaled mass to receive 100 mrem (g)
²³⁸ U	D	3.89E-06	1.29E+06	2.57E+04
	W	3.32E-06	1.51E+06	3.02E+04
	Y	4.00E-05	1.25E+05	2.50E+03
²³² Th	W	1.81E-03	2.76E+03	5.52E+01
	Y	3.45E-04	1.45E+04	2.90E+02

Table A.2: Dose responsible for x mass in grams to be inhaled, ICRP 30

ICRP 30			DOSE RESPONSIBLE FOR MASS INHALED								
Radionuclide	Class	Dose per unit mass (rem g ⁻¹)	100 g Inhaled mass (rem)	10 g Inhaled mass (rem)	1 g Inhaled mass (rem)	100 mg Inhaled mass (rem)	10 mg Inhaled mass (rem)	1 mg Inhaled mass (rem)	100 ug Inhaled mass (rem)	10 ug Inhaled mass (rem)	1 ug Inhaled mass (rem)
²³⁸ U	D	3.89E-06	3.89E-04	3.89E-05	3.89E-06	3.89E-07	3.89E-08	3.89E-09	3.89E-10	3.89E-11	3.89E-12
	W	3.32E-06	3.32E-04	3.32E-05	3.32E-06	3.32E-07	3.32E-08	3.32E-09	3.32E-10	3.32E-11	3.32E-12
	Y	4.00E-05	4.00E-03	4.00E-04	4.00E-05	4.00E-06	4.00E-07	4.00E-08	4.00E-09	4.00E-10	4.00E-11
²³² Th	W	1.81E-03	1.81E-01	1.81E-02	1.81E-03	1.81E-04	1.81E-05	1.81E-06	1.81E-07	1.81E-08	1.81E-09
	Y	3.45E-04	3.45E-02	3.45E-03	3.45E-04	3.45E-05	3.45E-06	3.45E-07	3.45E-08	3.45E-09	3.45E-10

Table A.3: Mass inhaled to reach public and occupational limits, ICRP 60

ICRP 60			MASS INHALED TO REACH PUBLIC AND OCCPUATIONAL LIMITS	
Radionuclide	Class	Dose per unit mass (rem g ⁻¹)	Inhaled mass to receive 5 rem (g)	Inhaled mass to receive 100 mrem (g)
²³⁸ U	F	1.26E-06	3.96E+06	7.93E+04
	M	2.52E-06	1.98E+06	3.97E+04
	S	3.99E-05	1.25E+05	2.51E+03
²³² Th	M	9.03E-04	5.54E+03	1.11E+02
	S	2.10E-04	2.38E+04	4.76E+02

Table A.4: Dose responsible for x mass in grams to be inhaled, ICRP 30

ICRP 60			DOSE RESPONSIBLE FOR MASS INHALED								
Radionuclide	Class	Dose per unit mass (rem g ⁻¹)	100 g Inhaled mass (rem)	10 g Inhaled mass (rem)	1 g Inhaled mass (rem)	100 mg Inhaled mass (rem)	10 mg Inhaled mass (rem)	1 mg Inhaled mass (rem)	100 ug Inhaled mass (rem)	10 ug Inhaled mass (rem)	1 ug Inhaled mass (rem)
²³⁸ U	F	1.26E-06	1.26E-04	1.26E-05	1.26E-06	1.26E-07	1.26E-08	1.26E-09	1.26E-10	1.26E-11	1.26E-12
	M	2.52E-06	2.52E-04	2.52E-05	2.52E-06	2.52E-07	2.52E-08	2.52E-09	2.52E-10	2.52E-11	2.52E-12
	S	3.99E-05	3.99E-03	3.99E-04	3.99E-05	3.99E-06	3.99E-07	3.99E-08	3.99E-09	3.99E-10	3.99E-11
²³² Th	M	9.03E-04	9.03E-02	9.03E-03	9.03E-04	9.03E-05	9.03E-06	9.03E-07	9.03E-08	9.03E-09	9.03E-10
	S	2.10E-04	2.10E-02	2.10E-03	2.10E-04	2.10E-05	2.10E-06	2.10E-07	2.10E-08	2.10E-09	2.10E-10

Appendix B: ICRP 30 and 60 Dose Calculations with Activity Concentration for Size Correction

Table B.1: Mass inhaled to reach public and occupational limits with size correction, ICRP 30

ICRP 30			MASS INHALED TO REACH PUBLIC AND OCCPUATIONAL LIMITS	
Radionuclide	Class	Dose per unit mass (rem g ⁻¹)	Inhaled mass to receive 5 rem (g)	Inhaled mass to receive 100 mrem (g)
²³⁸ U	D	3.63E-06	1.38E+06	2.75E+04
	W	5.14E-06	9.73E+05	1.95E+04
	Y	8.00E-05	6.25E+04	1.25E+03
²³² Th	W	1.73E-03	2.89E+03	5.78E+01
	Y	6.00E-04	8.33E+03	1.67E+02

Table B.2: Dose responsible for x mass in grams to be inhaled with size correction, ICRP 30

ICRP 30			DOSE RESPONSIBLE FOR MASS INHALED								
Radionuclide	Class	Dose per unit mass (rem g ⁻¹)	100 g Inhaled mass (rem)	10 g Inhaled mass (rem)	1 g Inhaled mass (rem)	100 mg Inhaled mass (rem)	10 mg Inhaled mass (rem)	1 mg Inhaled mass (rem)	100 ug Inhaled mass (rem)	10 ug Inhaled mass (rem)	1 ug Inhaled mass (rem)
²³⁸ U	D	3.63E-06	3.63E-04	3.63E-05	3.63E-06	3.63E-07	3.63E-08	3.63E-09	3.63E-10	3.63E-11	3.63E-12
	W	5.14E-06	5.14E-04	5.14E-05	5.14E-06	5.14E-07	5.14E-08	5.14E-09	5.14E-10	5.14E-11	5.14E-12
	Y	8.00E-05	8.00E-03	8.00E-04	8.00E-05	8.00E-06	8.00E-07	8.00E-08	8.00E-09	8.00E-10	8.00E-11
²³² Th	W	1.73E-03	1.73E-01	1.73E-02	1.73E-03	1.73E-04	1.73E-05	1.73E-06	1.73E-07	1.73E-08	1.73E-09
	Y	6.00E-04	6.00E-02	6.00E-03	6.00E-04	6.00E-05	6.00E-06	6.00E-07	6.00E-08	6.00E-09	6.00E-10

Table B.3: Mass inhaled to reach public and occupational limits with size correction, ICRP 60

ICRP 60			MASS INHALED TO REACH PUBLIC AND OCCPUATIONAL LIMITS	
Radionuclide	Class	Dose per unit mass (rem g ⁻¹)	Inhaled mass to receive 5 rem (g)	Inhaled mass to receive 100 mrem (g)
²³⁸ U	F	1.20E-06	4.17E+06	8.33E+04
	M	4.40E-06	1.14E+06	2.27E+04
	S	8.00E-05	6.25E+04	1.25E+03
²³² Th	M	8.60E-04	5.81E+03	1.16E+02
	S	3.90E-04	1.28E+04	2.56E+02

Table B.4: Dose responsible for x mass in grams to be inhaled with size correction, ICRP 60

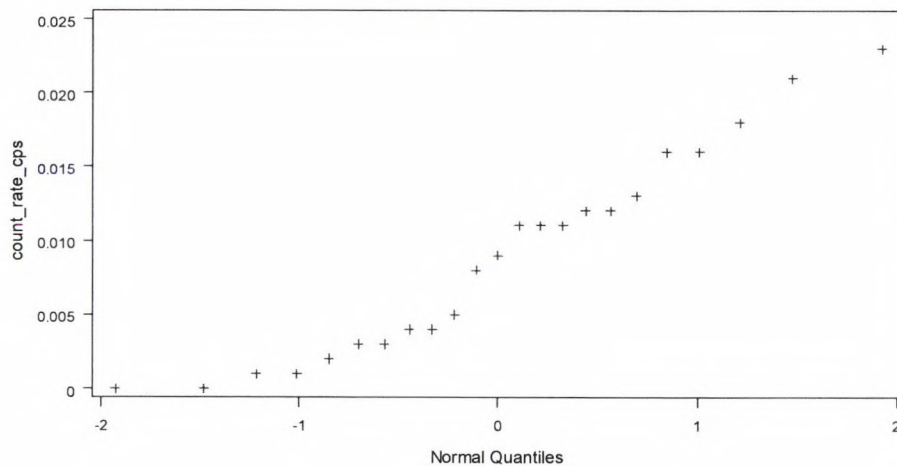
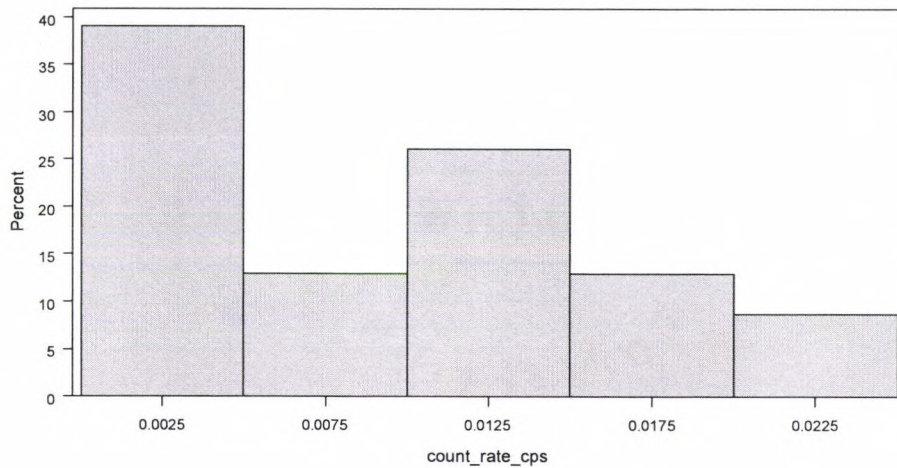
ICRP 60			DOSE RESPONSIBLE FOR MASS INHALED								
Radionuclide	Class	Dose per unit mass (rem g ⁻¹)	100 g Inhaled mass (rem)	10 g Inhaled mass (rem)	1 g Inhaled mass (rem)	100 mg Inhaled mass (rem)	10 mg Inhaled mass (rem)	1 mg Inhaled mass (rem)	100 ug Inhaled mass (rem)	10 ug Inhaled mass (rem)	1 ug Inhaled mass (rem)
²³⁸ U	F	1.20E-06	1.20E-04	1.20E-05	1.20E-06	1.20E-07	1.20E-08	1.20E-09	1.20E-10	1.20E-11	1.20E-12
	M	4.40E-06	4.40E-04	4.40E-05	4.40E-06	4.40E-07	4.40E-08	4.40E-09	4.40E-10	4.40E-11	4.40E-12
	S	8.00E-05	8.00E-03	8.00E-04	8.00E-05	8.00E-06	8.00E-07	8.00E-08	8.00E-09	8.00E-10	8.00E-11
²³² Th	M	8.60E-04	8.60E-02	8.60E-03	8.60E-04	8.60E-05	8.60E-06	8.60E-07	8.60E-08	8.60E-09	8.60E-10
	S	3.90E-04	3.90E-02	3.90E-03	3.90E-04	3.90E-05	3.90E-06	3.90E-07	3.90E-08	3.90E-09	3.90E-10

Appendix C: Gross Alpha Counting Tests for Normality using SAS software

LINEAR TRANSFORMATION (count_rate_cps)

Tests for Normality

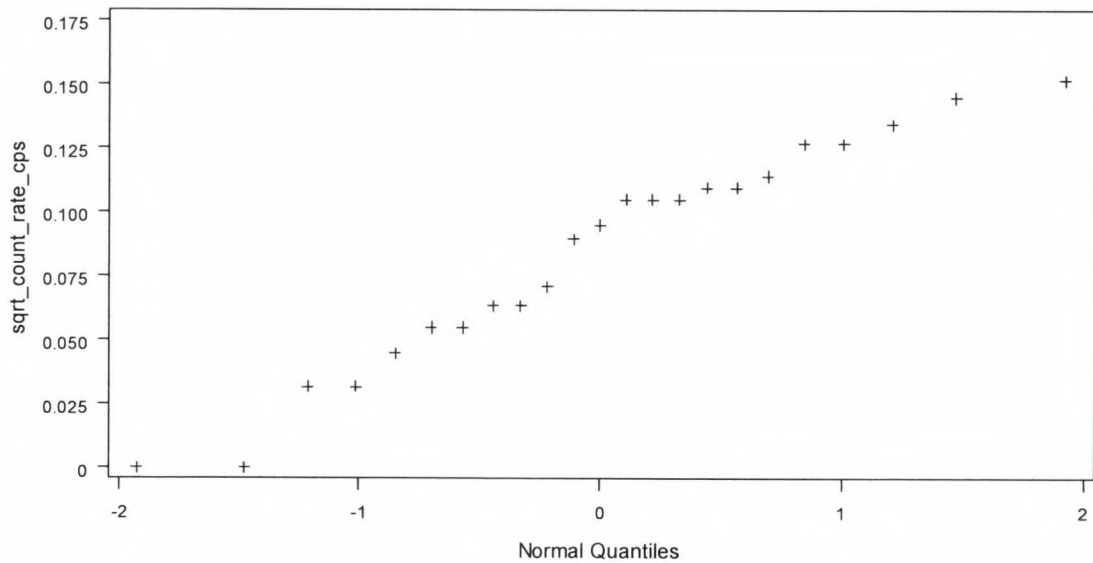
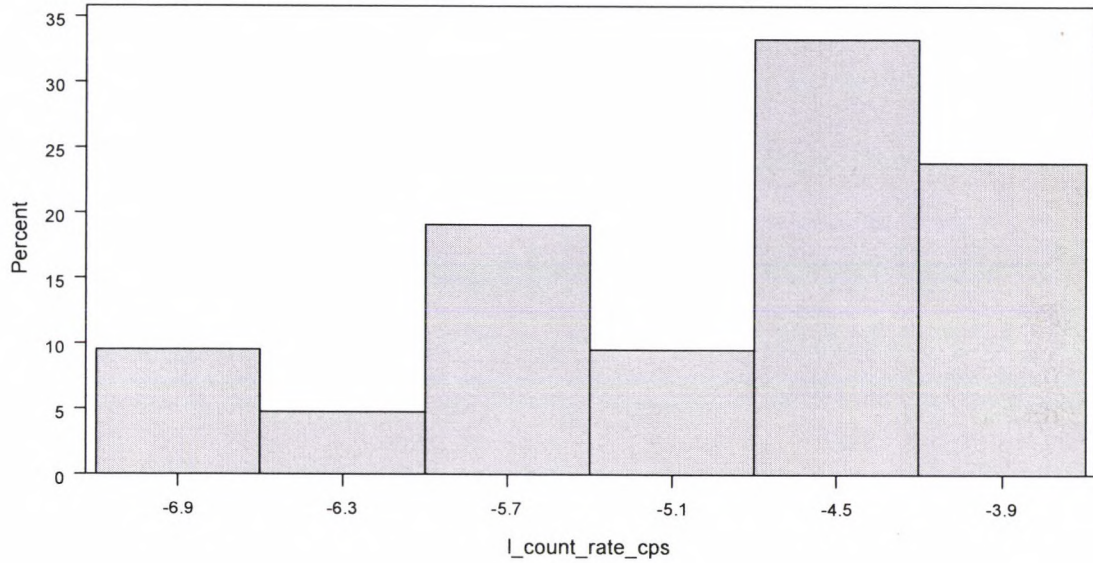
Test	--Statistic---	-----p Value-----
Shapiro-Wilk	W 0.935133	Pr < W 0.1412
Kolmogorov-Smirnov	D 0.151633	Pr > D >0.1500
Cramer-von Mises	W-Sq 0.075839	Pr > W-Sq 0.2295
Anderson-Darling	A-Sq 0.49304	Pr > A-Sq 0.2047



LOG TRANSFORMATION (l_count_rate_cps)

Tests for Normality

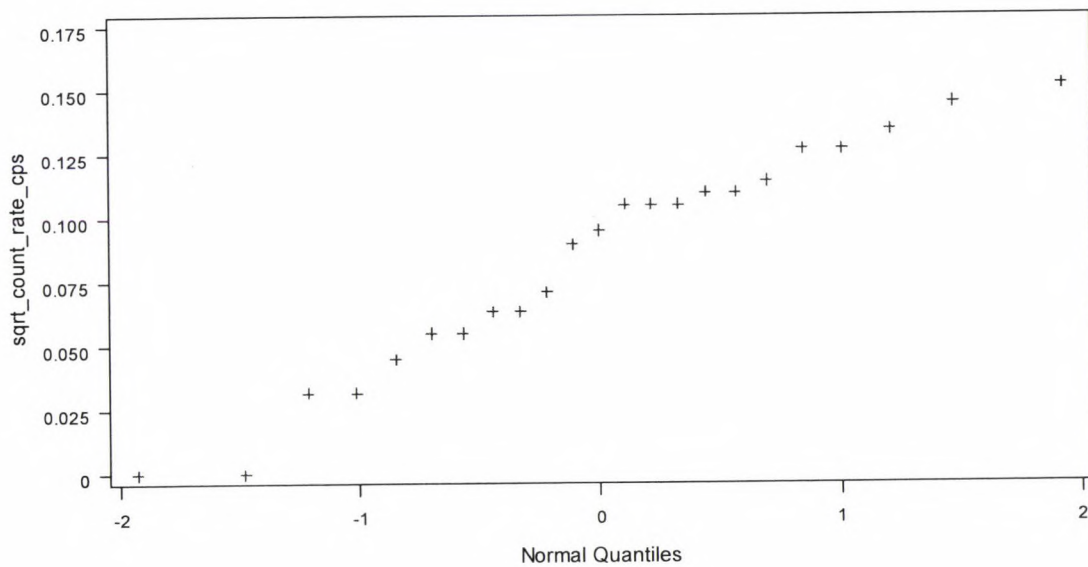
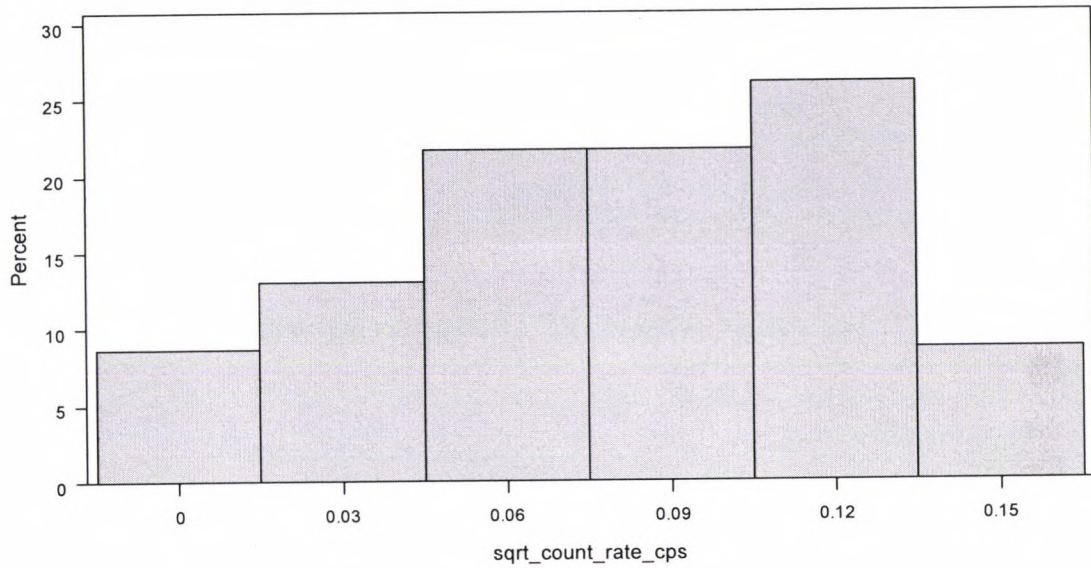
Test		--Statistic--		-----p Value-----
Shapiro-Wilk	W	0.901914	Pr < W	0.0381
Kolmogorov-Smirnov	D	0.207086	Pr > D	0.0193
Cramer-von Mises	W-Sq	0.133238	Pr > W-Sq	0.0382
Anderson-Darling	A-Sq	0.767178	Pr > A-Sq	0.0404



SQUARE ROOT TRANSFORMATION (sqrt_count_rate_cps)

Tests for Normality

Test	--Statistic---	-----p Value-----
Shapiro-Wilk	W 0.952558	Pr < W 0.3304
Kolmogorov-Smirnov	D 0.162504	Pr > D 0.1142
Cramer-von Mises	W-Sq 0.067608	Pr > W-Sq >0.2500
Anderson-Darling	A-Sq 0.391338	Pr > A-Sq >0.2500



SAS CODE

```
data alpha_mass_calibration;
input count_rate_cps @@;
datalines;
0.001
0.003
0.004
0.005
0.001
0.000
0.002
0.000
0.008
0.003
0.004
0.012
0.013
0.009
0.011
0.016
0.011
0.018
0.012
0.011
0.016
0.023
0.021
;
proc sort;
by count_rate_cps;
proc print;
var count_rate_cps;
proc univariate normal;
var count_rate_cps;
histogram count_rate_cps;
qqplot count_rate_cps;
run;
data alpha_mass_calibration;
set alpha_mass_calibration;
l_count_rate_cps=log(count_rate_cps);
proc sort;
by l_count_rate_cps;
proc print;
var l_count_rate_cps;
proc univariate normal;
var l_count_rate_cps;
histogram l_count_rate_cps;
qqplot l_count_rate_cps;
run;
data alpha_mass_calibration;
set alpha_mass_calibration;
sqrt_count_rate_cps=sqrt(count_rate_cps);
proc sort;
by sqrt_count_rate_cps;
proc print;
var sqrt_count_rate_cps;
```

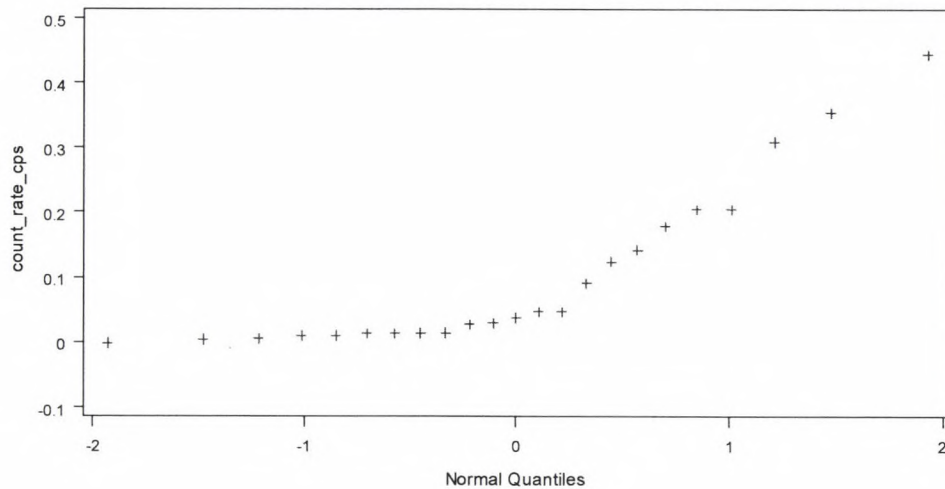
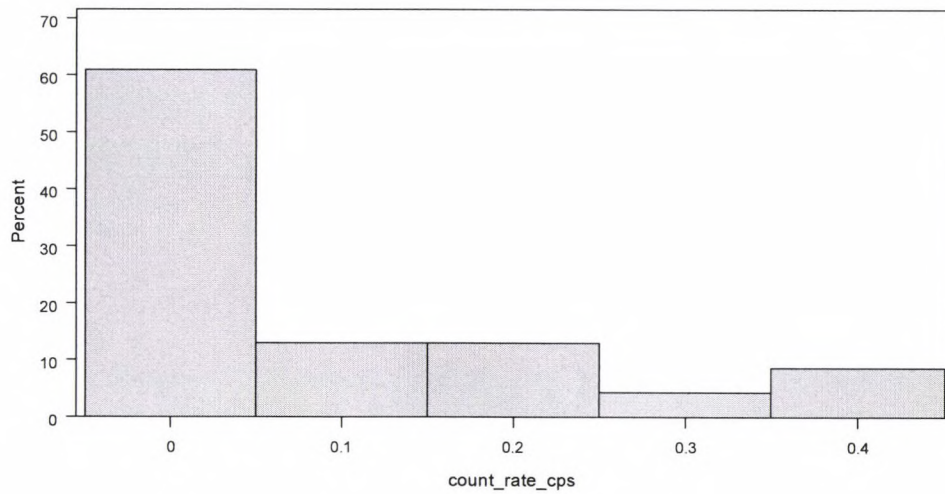
```
proc univariate normal;  
var sqrt_count_rate_cps;  
histogram sqrt_count_rate_cps;  
qqplot sqrt_count_rate_cps;  
run;
```

Appendix D: Gross Beta Counting Tests for Normality using SAS software

LINEAR TRANSFORMATION (count_rate_cps)

Tests for Normality

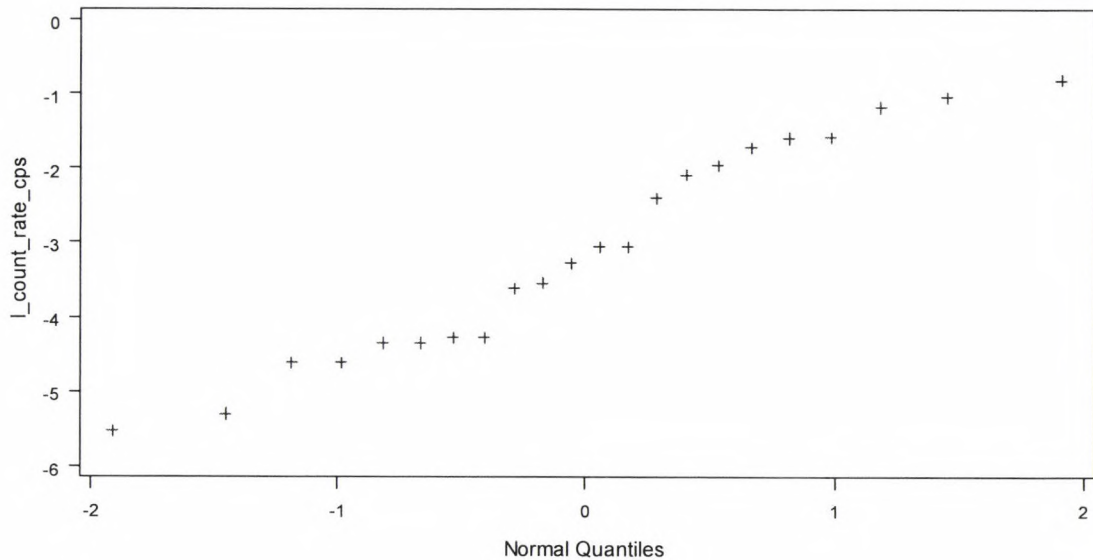
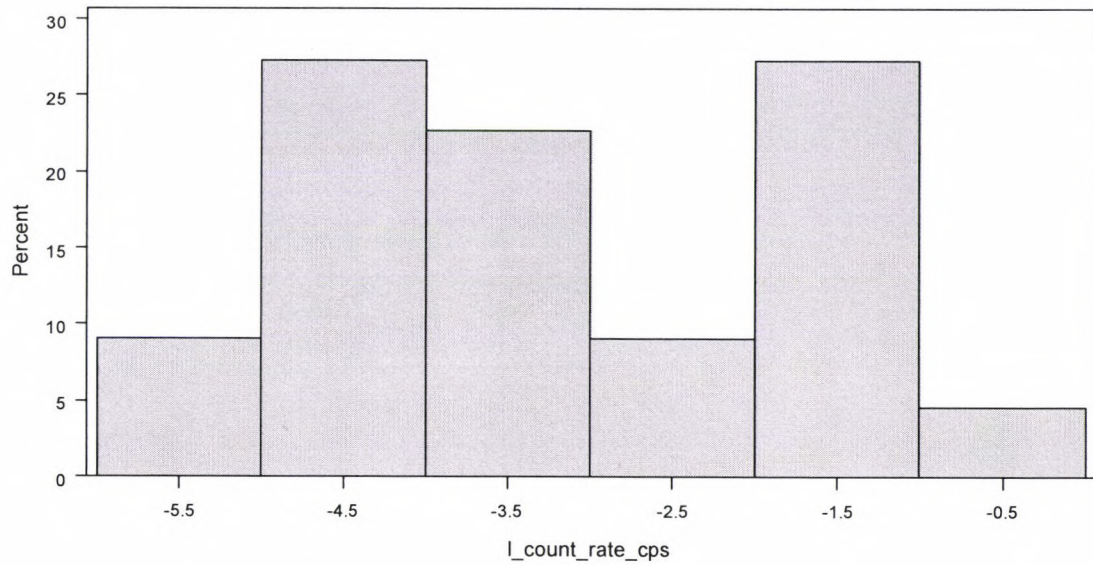
Test	--Statistic--	-----p Value-----
Shapiro-Wilk	W 0.779112	Pr < W 0.0002
Kolmogorov-Smirnov	D 0.273805	Pr > D <0.0100
Cramer-von Mises	W-Sq 0.352674	Pr > W-Sq <0.0050
Anderson-Darling	A-Sq 1.978416	Pr > A-Sq <0.0050



LOG TRANSFORMATION (l_count_rate_cps)

Tests for Normality

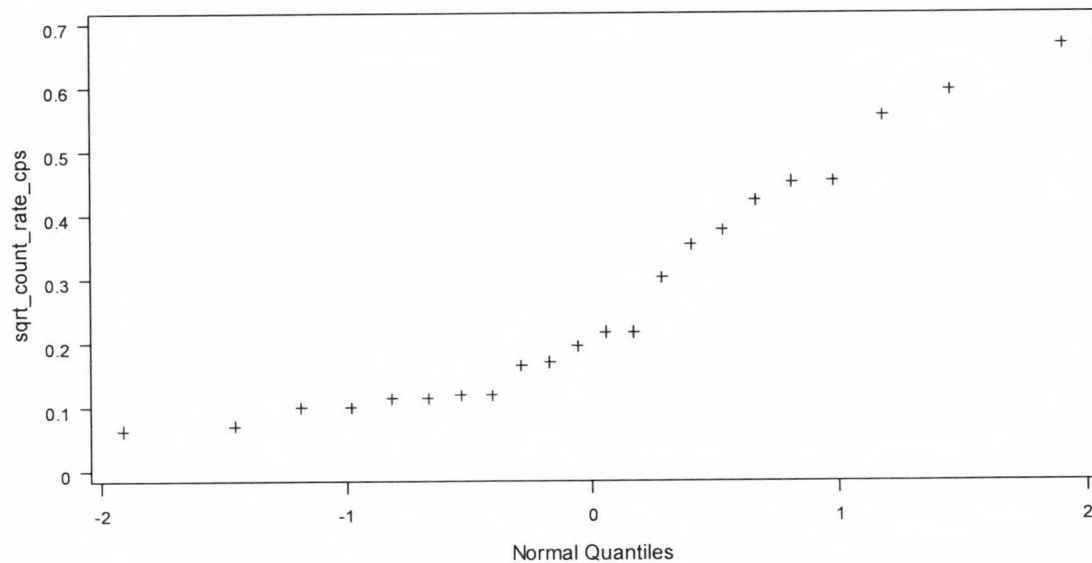
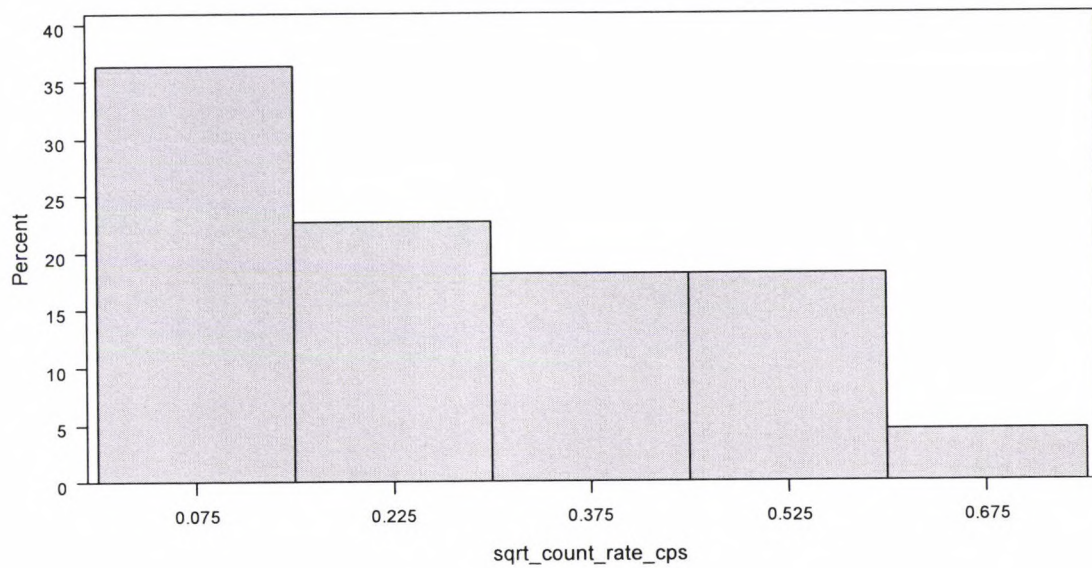
Test		--Statistic---		-----p Value-----
Shapiro-Wilk	W	0.943435	Pr < W	0.2328
Kolmogorov-Smirnov	D	0.154272	Pr > D	>0.1500
Cramer-von Mises	W-Sq	0.073553	Pr > W-Sq	0.2428
Anderson-Darling	A-Sq	0.456771	Pr > A-Sq	0.2451



SQUARE ROOT TRANSFORMATION (sqrt_count_rate_cps)

Tests for Normality

Test		--Statistic---		-----p Value-----
Shapiro-Wilk	W	0.886225	Pr < W	0.0159
Kolmogorov-Smirnov	D	0.203653	Pr > D	0.0184
Cramer-von Mises	W-Sq	0.162259	Pr > W-Sq	0.0160
Anderson-Darling	A-Sq	0.946882	Pr > A-Sq	0.0148



SAS CODE

```
data beta_mass_calibration;
input count_rate_cps @@;
datalines;
0.005
0.010
0.014
0.027
0.013
0.004
0.013
0.010
0.029
0.014
-0.002
0.047
0.038
0.047
0.142
0.091
0.124
0.179
0.204
0.205
0.309
0.354
0.444
;
proc sort;
by count_rate_cps;
proc print;
var count_rate_cps;
proc univariate normal;
var count_rate_cps;
histogram count_rate_cps;
qqplot count_rate_cps;
run;
data beta_mass_calibration;
set beta_mass_calibration;
l_count_rate_cps=log(count_rate_cps);
proc sort;
by l_count_rate_cps;
proc print;
var l_count_rate_cps;
proc univariate normal;
var l_count_rate_cps;
histogram l_count_rate_cps;
qqplot l_count_rate_cps;
run;
data beta_mass_calibration;
set beta_mass_calibration;
sqrt_count_rate_cps=sqrt(count_rate_cps);
proc sort;
by sqrt_count_rate_cps;
proc print;
var sqrt_count_rate_cps;
```

```
proc univariate normal;  
var sqrt_count_rate_cps;  
histogram sqrt_count_rate_cps;  
qqplot sqrt_count_rate_cps;  
run;
```

Appendix E: Gross Alpha Counting Regression Tests using SAS software

LINEAR TRANSFORMATION WITH LINEAR REGRESSION AUTOCORRELATION (count_rate_cps vs. mass_mg)

The ARIMA Procedure

Name of Variable = ry

Mean of Working Series -187E-20
Standard Deviation 0.004339
Number of Observations 23

Autocorrelations

Lag	Covariance	Correlation	-1	9	8	7	6	5	4	3	2	1	0	1	2	3	4	5	6	7	8	9	1	Std Error
0	0.00001883	1.00000												*****										0
1	8.69977E-6	0.46203							.					*****										0.208514
2	7.54018E-6	0.40044							.					*****										0.249080
3	9.0593E-6	0.48112							.					*****										0.275653
4	4.51548E-6	0.23981							.					*****										0.310021
5	1.26728E-6	0.06730							.					*****										0.317984

"." marks two standard errors

Inverse Autocorrelations

Lag	Correlation	-1	9	8	7	6	5	4	3	2	1	0	1	2	3	4	5	6	7	8	9	1	
1	-0.10676								.		**												
2	-0.16573								.		***												
3	-0.33751								.		*****												
4	-0.00912								.														
5	0.17781								.				****										

Partial Autocorrelations

Lag	Correlation	-1	9	8	7	6	5	4	3	2	1	0	1	2	3	4	5	6	7	8	9	1	
1	0.46203								.				*****										
2	0.23772								.				*****	.									
3	0.31028								.				*****	.									
4	-0.13263								.		***												
5	-0.23843								.		*****												

LINEAR TRANSFORMATION WITH NON-LINEAR REGRESSION AUTOCORRELATION (count_rate_cps vs. mass_mg)

The ARIMA Procedure

Name of Variable = rcr

Mean of Working Series 0.000367
Standard Deviation 0.003252
Number of Observations 23

Autocorrelations

Lag	Covariance	Correlation	-1	9	8	7	6	5	4	3	2	1	0	1	2	3	4	5	6	7	8	9	1	Std Error	
0	0.00001057	1.00000													*****									0	
1	2.51624E-6	0.23795							.						*****	.									0.208514
2	-1.5739E-6	-.14883							.		***					.									0.220004
3	-5.9525E-8	-.00563							.							.									0.224338
4	-3.0257E-7	-.02861							.			*				.									0.224345
5	-4.2806E-7	-.04048							.			*				.									0.224503

"," marks two standard errors

Inverse Autocorrelations

Lag	Correlation	-1	9	8	7	6	5	4	3	2	1	0	1	2	3	4	5	6	7	8	9	1			
1	-0.38206									*****						.									
2	0.28537								.						*****	.									
3	-0.13989								.		***					.									
4	0.08723								.				**			.									
5	-0.00926								.							.									

Partial Autocorrelations

Lag	Correlation	-1	9	8	7	6	5	4	3	2	1	0	1	2	3	4	5	6	7	8	9	1			
1	0.23795								.						*****	.									
2	-0.21778								.		****					.									
3	0.09939								.						**	.									
4	-0.09801								.			**				.									
5	0.01117								.							.									

LOG TRANSFORMATION WITH LINEAR REGRESSION
 AUTOCORRELATION
 (l_count_rate_cps vs. mass_mg)

The ARIMA Procedure

Name of Variable = ry

Mean of Working Series 1.08E-15
 Standard Deviation 0.446073
 Number of Observations 23
 Embedded missing values in working series 2

Autocorrelations

Lag	Covariance	Correlation	-1	9	8	7	6	5	4	3	2	1	0	1	2	3	4	5	6	7	8	9	1	Std Error
0	0.198981	1.00000											*****											0
1	-0.0086355	-.04340										*												0.208514
2	-0.035660	-.17921										****												0.208907
3	-0.048594	-.24421										****												0.215488
4	-0.0093604	-.04704										*												0.227203
5	0.0040357	0.02028										.												0.227626

"," marks two standard errors

Inverse Autocorrelations

Lag	Correlation	-1	9	8	7	6	5	4	3	2	1	0	1	2	3	4	5	6	7	8	9	1	
1	0.27008										.		*****	.									
2	0.30445										.		*****	.									
3	0.29482										.		*****	.									
4	0.13482										.		***	.									
5	0.09059										.		**	.									

Partial Autocorrelations

Lag	Correlation	-1	9	8	7	6	5	4	3	2	1	0	1	2	3	4	5	6	7	8	9	1	
1	-0.04340										*												
2	-0.18144										****												
3	-0.27068										*****												
4	-0.13226										***												
5	-0.11010										**												

SAS CODE

```
data alpha_mass_calibration;
input count_rate_cps mass_mg;
mass_sq = mass_mg*mass_mg;
datalines;
0.001 1.4
0.003 3.2
0.004 4.1
0.005 5.6
0.001 7.2
0.000 11
0.002 13.2
0.000 19.6
0.008 44
0.003 63.1
0.004 57.2
0.012 118.9
0.013 152.2
0.009 142.5
0.011 650.5
0.016 525.9
0.011 530.8
0.018 1039.6
0.012 1119.5
0.011 1452.2
0.016 2443
0.023 3379
0.021 5115
;
proc sort; by mass_mg;
run;
proc reg alpha=0.05;
model count_rate_cps=mass_mg /r clm cli;
plot count_rate_cps*mass_mg /pred;
output out = apyandry predicted = py residual = ry lcl = lci ucl
=uci lclm = llm uclm = ulm;
run;

data _NULL_; set apyandry;
file 'G:\Thesis\SAS codes\test2.txt' dlm='09'X;

put mass_mg count_rate_cps py ry lci uci llm ulm;

run;

proc plot;
plot count_rate_cps * mass_mg = '*' py * mass_mg = 'p' / overlay;
plot ry*mass_mg / vref=0;
run;

proc arima;
identify var = ry;
run;
proc glm;
model count_rate_cps = mass_mg mass_sq / solution;
run;
```

```

proc nlin method = gauss maxiter = 200;
parameters

a=0.015 to 0.025 by 0.0010

b=0.1 to 0.3 by 0.02;
model count_rate_cps = a*(1-exp(-b*mass_mg));
output out=asymp predicted = pcr residual = rcr;
data _NULL_; set asymp;
file 'G:\Thesis\SAS codes\test5.txt' dlm='09'X;

put mass_mg count_rate_cps pcr rcr;

run;

proc arima;
identify var = rcr;
run;

proc plot;
plot pcr*mass_mg = 'p' count_rate_cps*mass_mg = '.' /overlay;
plot rcr*mass_mg / vref = 0;
run;
proc plot;
plot count_rate_cps*mass_mg;
run;
data alpha_mass_calibration;
set alpha_mass_calibration;
l_count_rate_cps=log(count_rate_cps);
l_mass_mg=log(mass_mg);

proc reg alpha=0.05;
model l_count_rate_cps=l_mass_mg /r clm cli;
plot l_count_rate_cps*l_mass_mg /pred;
output out = pyandry predicted = py residual = ry lcl = lci ucl =uci
lclm = llm uclm = ulm;
run;
data _NULL_; set pyandry;
file 'G:\Thesis\SAS codes\test3.txt' dlm='09'X;

put l_mass_mg l_count_rate_cps py ry lci uci llm ulm;

run;
proc plot;
plot ry*l_mass_mg / vref=0;
run;
proc sort; by mass_mg;
run;
proc arima;
identify var = ry;
run;

```


Appendix F: Gross Beta Counting Regression Tests using SAS software

SAS CODE

```
data beta_mass_calibration;
input count_rate_cps mass_mg;
mass_sq=mass_mg*mass_mg;
datalines;
0.005 1.4
0.010 3.2
0.014 4.1
0.027 5.6
0.013 7.2
0.004 11
0.013 13.2
0.010 19.6
0.029 44
0.014 63.1
-0.002 57.2
0.047 118.9
0.038 152.2
0.047 142.5
0.142 650.5
0.091 525.9
0.124 530.8
0.179 1039.6
0.204 1119.5
0.205 1452.2
0.309 2443
0.354 3379
0.444 5115
;
proc reg alpha=0.05;
model count_rate_cps=mass_mg/r clm cli;
plot count_rate_cps*mass_mg /pred;
output out = linpyandry predicted = lin_py residual = lin_ry;
run;
proc plot;
plot lin_ry*mass_mg / vref=0;
run;

proc glm;
model count_rate_cps = mass_mg mass_sq / solution;
run;

data beta_mass_calibration;
set beta_mass_calibration;
l_count_rate_cps=log(count_rate_cps);
l_mass_mg=log(mass_mg);

proc reg alpha=0.05;
model l_count_rate_cps=l_mass_mg /r clm cli;
plot l_count_rate_cps*l_mass_mg /pred;
output out = pyandry predicted = py residual = ry lcl = lci ucl =uci
lclm = llm uclm = ulm;
run;
```

```
data _NULL_ ; set pyandry;
file 'G:\Thesis\SAS codes\test4.txt' dlm='09'X;

put l_mass_mg l_count_rate_cps py ry lci uci llm ulm;

run;
proc plot;
plot ry*mass_mg / vref=0;
run;
```

Appendix G: Size Adjustment Calculations

$$\% \text{ increase}_{\text{between size bins}} = \frac{|\text{concentration}_{\text{original}} - \text{concentration}_{\text{new}}|}{\text{concentration}_{\text{original}}} \times 100$$

For example:

$$\% \text{ increase}_{7-10\mu\text{m}} = \frac{\left| 539 \frac{\text{Bq}}{\text{kg}} - 604 \frac{\text{Bq}}{\text{kg}} \right|}{539 \frac{\text{Bq}}{\text{kg}}} \times 100 = 14\%$$

Table G.1: Size adjustment calculations for ²³⁸U

size (μm)	% increase between size bins	Activity Concentration (pCi g ⁻¹)	Corrected Activity Concentration (pCi g ⁻¹)
1	0.33	0.48	3.54
3	0.27	1.03	2.66
5	0.14	1.33	2.09
10, 14, 20	0	1.87	1.87

Table G.2: Size adjustment calculations for ²³²Th

size (μm)	% increase between size bins	Activity Concentration (pCi g ⁻¹)	Corrected Activity Concentration (pCi g ⁻¹)
1	0.03	0.33	2.07
3	0.09	0.65	2.01
5	0.14	0.76	1.84
10, 14, 20	0	1.61	1.61

**Appendix H:
Copyright Permission**



January 11, 2010

Felicity Cunningham Beckfield
Health Physics Graduate Student
Colorado State University
Fort Collins, Colorado 80523

Dear Ms. Beckfield,

This is in response to your request to reprint graphics depicting coal formation and coal rank found at the website of the Kentucky Geological Survey. You have indicated that you want to use these images as pictorial representations in your master's thesis.

Permission is granted for this use with the understanding that appropriate credit will be given to the Kentucky Geological Survey and to Stephen Greb of KGS, who created the graphics.

Thank you for your interest in KGS and information on our website.

Regards,

A handwritten signature in black ink that reads 'Mike Lynch'. The signature is written in a cursive style with a large, sweeping 'M' and a long, trailing 'y'.

Mike Lynch
Communications and Technology

Transfer

(859) 323-0561
mike.lynch@uky.edu